THE UNIVERSITY OF MICHIGAN
OFFICE OF RESEARCH ADMINISTRATION
ANN ARBOR

AN ANALYSIS OF THE BRETT ULTRA-WIDEBAND VIDEO AMPLIFIER

Technical Report No. 122

2899-55-T

Cooley Electronics Laboratory
Department of Electrical Engineering

By: D. K. Adams

Approved by: B. F. Barton

Project 2899

Task Order No. EDG-4
Contract No. DA-36-039 sc-78283
Signal Corps, Department of the Army
Department of the Army Project No. 3A99-06-001-01

July 1961

ABSTRACT

A detailed analysis is made of the process of phase modulation by a nonlinear reactance element. This analysis is applied to a video amplifier circuit developed by Mr. H. Brett of the U. S. Army Signal Research and Development Laboratory and shows this circuit to be capable of ultra-wideband amplification. The basic mechanism for this amplification is discussed in terms of several analytical viewpoints, which are ultimately shown to be consistent.

Formulas for all basic circuit quantities are derived, including gain, bandwidth, input and output impedance, and noise figure. This analysis is used to predict optimum design techniques when nonideal components are incorporated in the Brett circuit. An illustrative design is given for a video amplifier with 20 db gain, 100 Mc bandwidth (0 to 100 Mc), and a noise figure of less than 0.1 db.

TABLE OF CONTENTS

LIST OF ILLUSTRATIONS

LIST OF SYMBOLS

Frequency Variables:		Defined or first used on page
f_s	applied (video) signal frequency	6
ω_s	$2\pi f_s$	6
y	$\omega_s t$	8
p	$\omega_s (\beta_s \beta_o)^{-\frac{1}{2}}$	51
f_o	local oscillator or pump frequency	6
ω_o	$2\pi f_o$	6
x	$\omega_o t$	8
q	$\omega_o (\beta_s \beta_o)^{-\frac{1}{2}}$	51
f_n	$f_o + nf_s$; $n = 0, \pm 1, \pm 2, \ldots$	7
ω_n	$2\pi f_n$	7
z	f_s/f_o	10
ω_D	angular frequency where varactor Q is unity	37
Current Variables:		
$i(t)$	total current flowing through the varactor, or through any of its representations	8
$i_o(t)$	waveform of applied pump current	8
I_s, I_n	complex Fourier amplitudes of components of $i(t)$ at f_s and f_n, respectively	6,8
I_{so}, I_{no}	complex Fourier amplitudes of applied current source at f_s and f_n, respectively	6,8
$i_C(t)$	waveform of current through C	8
$i_L(t)$	waveform of current through L	9
$i_{sc}(t)$	waveform of short circuit current	18

Voltage Variables:		Defined or first used on page
$V(t)$	waveform of total varactor voltage	18
$v(t)$	time-varying portion of $V(t)$	18
$\overline{V}$	dc portion of $V(t)$	18
$v(t)$	waveform of voltage across $c_s(t)$	6
V_s, V_n	complex Fourier amplitudes of components of $V(t)$ at f_s and f_n, respectively	6,7
Φ	angular deviation of phase modulation	6
Φ_o, $\overline{V}_o$	phase and amplitude, respectively of V_o	11
S	see (20b)	11
B, θ	amplitude and phase, respectively, of correlating signal for phase detection	13
$A(t)$, $\varphi(t)$	envelope and phase, respectively, of $V(t)$	13
$M(t)$, $\psi(t)$	envelope and phase, respectively, of composite signal (sum of (25) and (26)	13
J_n	nth order Bessel function of 1st kind	7
Time-Varying Capacitance Variables:		
$c_s(t)$	waveform of capacitance varying harmonically at f_s	5
C_s	complex Fourier amplitude of $c_s(t)$	6,8
$c_o(t)$	waveform of capacitance varying harmonically at f_o	23
C_o	complex Fourier amplitude of $c_o(t)$	23

Circuit Elements and Parameters:		Defined or first used on page
C	total shunt capacitance in pump circuit	6
L	total shunt inductance in pump circuit	6
L, C_B	high pass filter in pump circuit	25
L_v, C_v	low pass filter in video circuit	25
G	total shunt conductance appearing in pump circuit	6
$C_T(V)$, Q(V)	capacitance and change characteristics, respectively, of a varactor	18,21
m, V_c, Q'	parameters characterizing Q(V)	34
$\overline{C}$	$C_T(\overline{V})$	
h_1, h_2	first and second order Taylor coefficients of $C_T(V)$	20
η_1 η_2	first and second order Taylor coefficients of Q(V)	20
G_s	internal conductance of video source	25
G_D	effective shunt conductance of varactor	37
G_L	effective shunt conductance reflected into pump circuit by external circuit	38
B_n	susceptance of pump circuit at f_n	9
Y_n	admittance of pump circuit at f_n	9
R	varactor series resistance	37
Q	varactor quality factor	10
$Y_{s_{IN}}$, $Y_{n_{IN}}$	total input admittance at f_s and f_n, respectively	26

Circuit Elements and Parameters (Cont.)		Defined or first used on page
$Y_{\ell n}$	transfer admittance from f_n to f_ℓ; ℓ = integer	43
α	pumping parameter (sec 51c)	29
r	C_s/C	10
Power and Gain Variables:		
P_{sb}	total sideband power delivered to G	12
P_s	total sideband power delivered by video source	12
$(TG)_{sn}$	transducer gain from f_s to f_n	28
$(TG)_s$	$\sum_n (TG)_{sn}$	28
$(TG)_0$	$(TG)_s$ evaluated $f_s \to 0$	29
(GB)	voltage-gain-times-bandwidth product	31
Bandwidth Variables:		
β	total system bandwidth in radians/sec	29
β_s	bandwidth of input video circuit in radians/sec	29
β_o	half-bandwidth of pump circuit in radians/sec	29
β_D	portion of β_o due to varactor loss	38
β_L	portion of β_o due to output load	38
B_{o_N}	noise bandwidth of pump circuit in cps	45
B_N	amplifier noise bandwidth in cps	42
Noise Variables:		
F	noise figure	42
N_s	excess noise power originating in video band	42

Noise Variables (Cont.)		Defined or first used on page
N_o	excess output noise power originating in pump band	42
K	Boltzmann's constant	42
T	room temperature	42
T'	noise temperature of G	43
T_D, T_L	noise temperature of G_D and G_L, respectively	43
di_N	increment of RMS noise current in interval $d\omega_s$	43
P_G	total noise power delivered to G	43

COOLEY ELECTRONICS LABORATORY TECHNICAL REPORT NO. 122

AN ANALYSIS OF THE BRETT ULTRA-WIDEBAND VIDEO AMPLIFIER

1. INTRODUCTION

The recent revival of engineering interest in reactive mixers, particularly in applications calling for low-noise energy conversion and amplification, has led to a wide variety of reactive-mixer circuits. This apparent versatility in reactive mixer design, when compared to that in conventional resistive mixers, can be attributed largely to the radical difference that occurs between the reactive-mixer sideband and its image. The nature of this dissimilarity is demonstrated in Fig. 1, which shows a typical frequency distribution of power for a double-sideband reactive mixer. The following features of Fig. 1 are noteworthy (Refs. 1 and 2):

(1) The output power in either or both of the sidebands can exceed the input signal power.

(2) The amounts of output power from these sidebands are typically unequal.

(3) The reflected power at the signal frequency may greatly exceed the input power.

Notes (1) and (2) above have been the basis of recent developments in low-noise microwave modulators and converters, while Note (3) is the basis of parametric amplification. In each of these applications, however, the emphasis to date has been on single-sideband circuits. This specialization has been motivated, at least in part, by the following factors:

(1) The greatest need for improved low-noise energy conversion has existed at microwave frequencies, but in this application practical factors also limit the local oscillator (i.e., the power source or pump) frequency to the microwave region. Therefore, the sidebands tend to have large frequency separations, and single-sideband operation is natural.

(2) For single-sideband converters operating on microwave signals, lower-sideband energy conversion tends to yield greater gain for a given noise figure (Ref. 3).

(3) If the output power is derived from only one sideband, any coupling to other sidebands tends to degrade circuit performance by introducing excess noise.

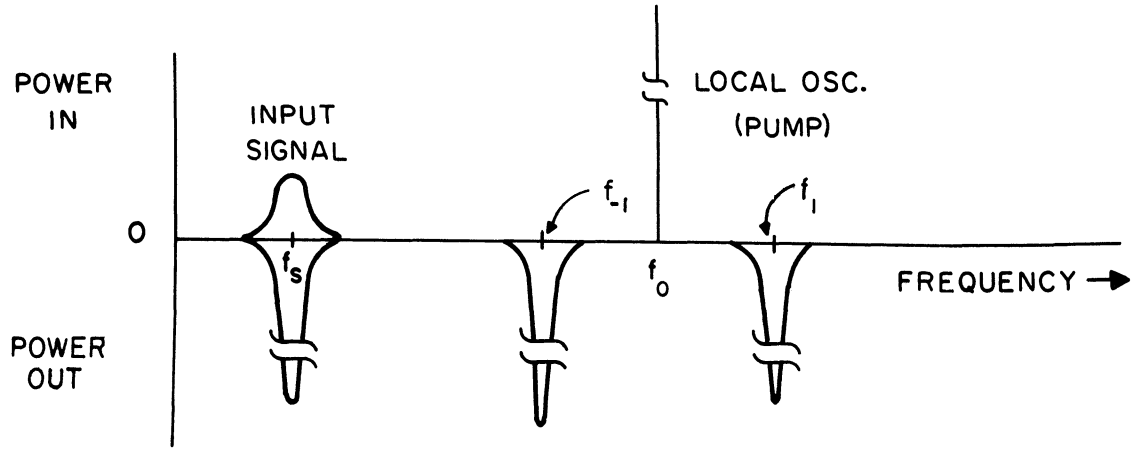

Fig. 1. Power distribution for a typical double-sideband reactive mixer.

It should be recognized that the factors cited above have historical importance but are insufficient to justify an exclusive interest in single-sideband reactive mixers. In fact, work at this laboratory has previously shown that double-sideband circuits can be designed to yield improved converter performance, even at microwave frequencies (Ref. 4).

Thus multiple-frequency reactive mixers are of justifiable engineering interest.

The purpose of this report is to extend the theory of reactive mixers to a particular multiple-sideband pattern associated with angular modulation. This analysis has been motivated by interesting experimental work conducted by Mr. H. Brett of the U. S. Army Signal Research and Development Laboratory (Ref. 5). The theory derived will be applied specifically to the Brett mixer-amplifier circuit shown in Fig. 2, which will be referred to hereafter as a parametric video amplifier.[+] In Fig. 2, a local oscillator signal at a frequency near 1500 Mc is applied to arm 1 of a hybrid junction and splits between arms 3 and 4. The signal emerging from arm 3 mixes with an applied video signal through the action of a nonlinear capacitor (varactor). This process will be shown to reflect back to arm 3 of the hybrid junction what is essentially a phase-modulated signal. At the same time the signal emerging at port 4 is reflected by an adjustable short. The two reflected signals now add in the hybrid, such that in-phase frequency components pass out arm 1, while out-of-phase components emerge from arm 2. Similarly, quadrature components divide equally in power between the two ports.

Brett reports that the detected and filtered signal on arm 2 is an amplified version of the original video signal which appears to contain little excess noise. Noise figures of less than 2 db and video bandwidths that are roughly 1 percent of the pump frequency have been estimated. The goal of this analysis, then, is to attempt to explain the origin of these results and to suggest possible methods for extending the performance of Brett's circuit.

[+]In this report, the term video will be applied to the extended frequency range from dc to several hundred megacycles.

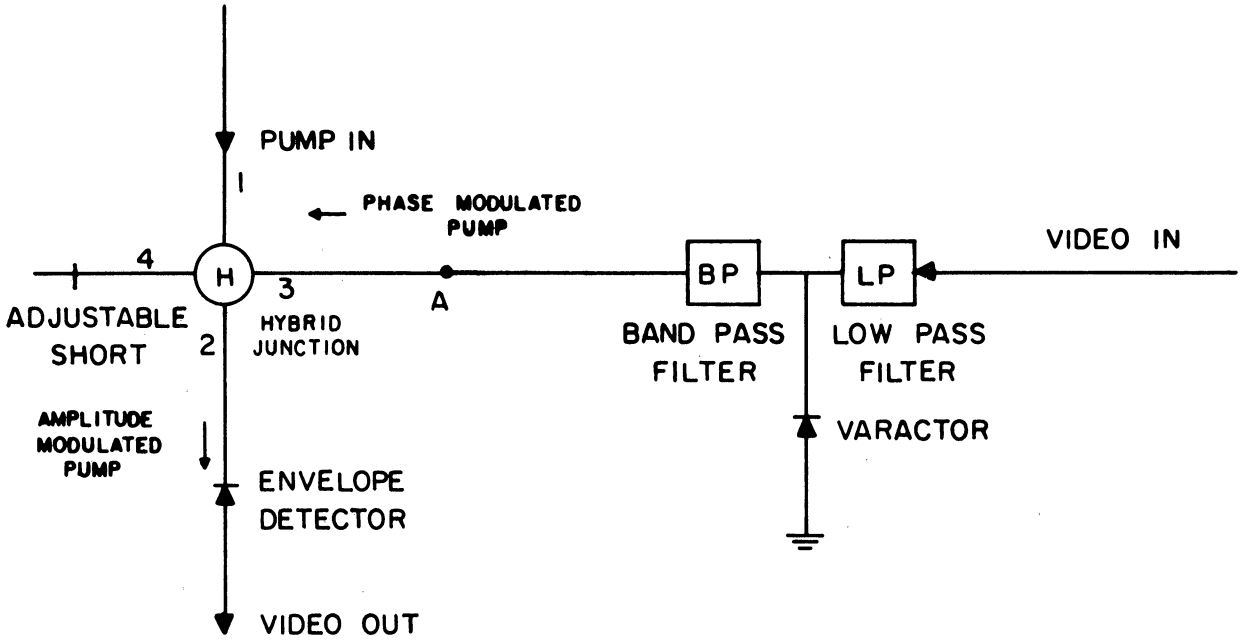

Fig. 2. Block diagram of the Brett Parametric Video Amplifier.

Since low-noise video amplification appears to be a property of the Brett circuit the analysis offered in this report will be concerned with small video signals. While a small signal analysis has limited applicability, it simplifies the mathematics in that the amplification process itself can be assumed linear. However, there appear to be at least two different ways for formulating this small-signal treatment. Perhaps the more conventional of these is to argue that the microwave signal, which is the power source (or pump) for video amplification, is much larger than the video signal, and therefore the varactor-plus-pump can be replaced by a time-varying capacitor at pump frequency. On the other hand, Brett has suggested that if the varactor-plus-video-signal is replaced by a time-varying capacitor at video frequency, the video signal can be imagined to angle modulate the pump. This report will demonstrate that these two approaches are consistent

with each other. Individually, however, they do tend to emphasize different aspects of parametric video amplification. Since the Brett concept of angle modulation by the video signal is the less conventional of the two, it will be treated first.

2. ANGLE MODULATION WITH TIME-VARYING CAPACITANCE

Traditionally, angle modulation is achieved either by varying the frequency of an oscillator (FM); or by splitting the output of an oscillator into two components, whose relative phase is shifted before they are recombined into a phase-modulated signal (Armstrong PM). In both of these systems the fundamental source of angle modulation is a circuit capable of presenting a varying reactance to the signal being modulated. In general this varying reactance is either an active circuit or is so closely allied with one that the energy conversion properties of the varying reactance are easily overlooked. For this reason, first attention will be devoted to an investigation of angle modulation by the time variation of a passive reactive component. In particular, the circuit in Fig. 3 will be considered and will be shown to illustrate a useful case of multiple-frequency reactive mixing. To relate Fig. 3 to the Brett circuit in Fig. 2, it is tentatively assumed that $c_s(t)$

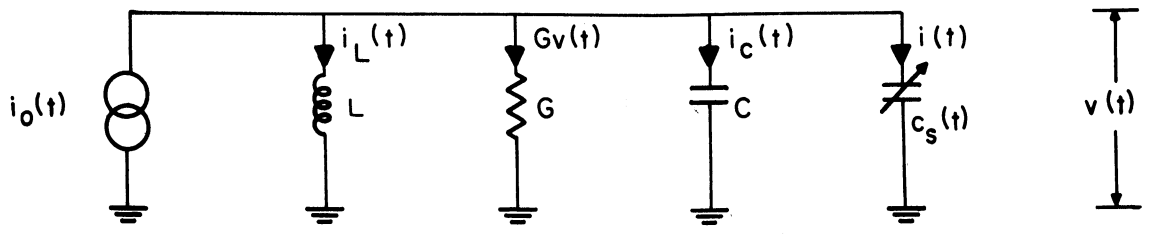

Fig. 3. A circuit for angle modulation by a time varying capacitance.

simulates everything to the right of the band-pass filter, the latter being represented by L and C. In Section 3, a more rigorous justification will be given for applying the analysis of this section to the Brett circuit.

In Fig. 3, a current at fixed frequency f_o is applied to the L-C circuit which is tuned to f_o, and is shunted by a capacitor varying harmonically in time at frequency f_s. (Note: This circuit is to be distinguished from that of a conventional FM modulator in which f_o is associated with a "loose", or tunable, oscillator). In the steady state, assuming

$$i_o(t) = I_{oo} \cos \omega_o t \tag{1a}$$

$$c_s(t) = C_s \sin \omega_s t \tag{1b}$$

this circuit will tend to produce a phase-modulated tank voltage that may be approximated by

$$v(t) = I_{oo} \cos (\omega_o t + \varphi \sin \omega_s t) \tag{2a}$$

where

$$\omega_o = 2\pi f_o \qquad \omega_s = 2\pi f_s \tag{2b}$$

The quantity φ is customarily termed the angular deviation, and quasi-static considerations suggest that:

$$\varphi \approx \tan^{-1} \frac{\omega_o C_s}{G} \ . \tag{2c}$$

The preceding expression for v(t) and φ have been cautiously stated, and indeed they will be shown to be inaccurate. For example, one obvious oversight in (1a) is incidental amplitude modulation. Other

more subtle discrepancies in (2a) and (2c) will be demonstrated.

It is instructive to consider the flow of energy in Fig. 3. Since charge is present on the time-varying capacitor, the latter can be expected to do work upon this charge. At the same time, modulation of the tank circuit voltage tends to draw extra power from the current source $i_o(t)$, so in this phase-modulation process energy may enter the circuit at both input frequencies. Thus, it can be anticipated that a suitable demodulator attached across the tank could recover an amplified version of the original f_s signal. The amplification in this case is due both to the power contributed by $i_o(t)$ to the modulation process and to the lossless character of the time-varying element. In the following paragraphs a quantitative evaluation of this effect will be presented.

2.1 A General Formulation of Angle Modulation with Time-Varying Capacitance

One well-known characteristic of (1a) is that it contains spectral components at all frequencies in the set $f_n = f_o + nf_s$, where $n = 0, \pm 1, \pm 2, \ldots$. This fact follows from the relation:

$$\cos(\omega_o t + \varphi \sin \omega_s t) = \sum_{n=-\infty}^{\infty} J_n(\varphi) \cos(\omega_n)t \qquad (3)$$

where $\omega_n = 2\pi f_n$ and $J_n(\varphi)$ is the nth-order Bessel function with the property that $J_{-n}(\varphi) = (-1)^n J_n(\varphi)$. In the steady state, v(t) in Fig. 3 will have the same spectral frequencies as (3), although the actual Fourier coefficients of v(t) will differ from those in (3) since v(t) is not simply sinusoidally phase-modulated. Therefore the following steady-state representation of v(t) will be taken.

$$v(t) = \mathrm{Re} \sum_{n=-\infty}^{\infty} V_n e^{j(x + ny)} \qquad 4)$$

where $x = 2\pi f_o t$ and $y = 2\pi f_s t$. From Fig. 3, this voltage must satisfy the equation

$$i_o(t) = i_c(t) + i_L(t) + Gv(t) + i(t) \tag{5}$$

where

$$i_o(t) = \mathrm{Re}(I_{oo} e^{jx}) \tag{6a}$$

$$c_s(t) = \mathrm{Re}(C_s e^{jy}) \tag{6b}$$

$$i(t) = \frac{d}{dt}\,[c_s(t)\, v(t)]. \tag{6c}$$

Note that the coefficients C_s and I_{oo} have now been made complex so the phases of $i_o(t)$ and $c_s(t)$ are arbitrary and are no longer restricted to those indicated in (1c). The subscript on $c_s(t)$ has been introduced to distinguish this time-varying capacitor from another that will be introduced in Section 3.

As a consequency of (5), i(t) will have the same spectral frequencies as v(t), or:

$$i(t) = \mathrm{Re} \sum_{n=-\infty}^{\infty} I_n e^{j(x + ny)} \tag{7}$$

Now, by employing (6c), these spectral components can be precisely related to the components of v(t), which yields the following basic result.

$$I_n = \frac{1}{2}\, j\omega_n \,(C_s V_{n-1} + C_s^* V_{n+1}) \tag{8}$$

Here, * denotes a complex conjugate. A final step prior to calculating the V_n through (5) is to note from Fig. 3 that

$$i_c(t) = \mathrm{Re} \sum_{n=-\infty}^{\infty} j\omega_n\, C V_n e^{j(x + ny)} \tag{9a}$$

$$i_L(t) = \mathrm{Re} \sum_{n=-\infty}^{\infty} \frac{V_n e^{j(x + ny)}}{j\omega_n L} \tag{9b}$$

Then using (4) and (9), (5) yields

$$I_o = GV_o + \frac{1}{2} j\omega_o (C_s V_{-1} + C_s^* V_1) \tag{10a}$$

$$0 = Y_n V_n + \frac{1}{2} j\omega_n (C_s V_{n-1} + C_s^* V_{n+1}); \quad n \neq 0 \tag{10b}$$

where (since $\omega_o^2 LC = 1$)

$$Y_n = G + jB_n \tag{11a}$$

$$B_n = \omega_n C - \frac{1}{\omega_n L} \approx 2n\omega_s C \tag{11b}$$

Therefore, given I_{oo} and C_s, the resulting $v(t)$ can be found if (10b) can be solved for the V_n.

It is instructive to write (10) in matrix form, as follows:

$$\begin{vmatrix} 0 \\ 0 \\ I_o \\ 0 \\ 0 \end{vmatrix} = \begin{vmatrix} \frac{1}{2}j\omega_{-2}C_s & Y_{-2} & \frac{1}{2}j\omega_{-2}C_s^* & & & \\ & \frac{1}{2}j\omega_{-1}C_s & Y_{-1} & \frac{1}{2}j\omega_{-1}C_s^* & & \\ & & \frac{1}{2}j\omega_o C_s & Y_o & \frac{1}{2}j\omega_o C_s^* & \\ & & & \frac{1}{2}j\omega_1 C_s & Y_1 & \frac{1}{2}j\omega_1 C_s^* \\ & & & & \frac{1}{2}j\omega_2 C_s & Y_2 & \frac{1}{2}j\omega_2 C_s^* \end{vmatrix} \begin{vmatrix} V_{-2} \\ V_{-1} \\ V_o \\ V_1 \\ V_2 \end{vmatrix} \tag{12}$$

A complete solution for $v(t)$ entails inverting the infinite matrix above which poses a difficult mathematical problem. However, approximate solutions have been obtained that are sufficiently enlightening for the present application.

If it is assumed that $v(t)$ is approximately representable by

(2), the magnitude of φ will never exceed $\pi/2$, so only the first three or four terms in (3) will ever be significant. Furthermore, if this circuit is employed as a phase modulator for small signals, the small-signal condition $|C_s/C| \ll 1$ can be imposed. In this case,

$$|\varphi| \approx \frac{\omega_o |C_s|}{G} = Q \left|\frac{C_s}{C}\right| \tag{13}$$

so the small-signal condition is more precisely given by

$$\left|\frac{C_s}{C}\right| \ll \frac{1}{Q} \tag{14}$$

When (14) is satisfied, all Fourier coefficients of v(t) should decrease rapidly with $|n|$. This assumption can be checked by neglecting all V_n in (12) except those for which $|n| \leq 2$ and solving (10) for the remaining sidebands. In support of the above statements, this calculation yields

$$\left|\frac{V_2}{V_o}\right| < Q^2 \left|\frac{C_s}{C}\right|^2; \quad \left|\frac{V_1}{V_o}\right| < Q \left|\frac{C_s}{C}\right| \tag{15}$$

Consequently, by imposing (14), all V_n except those with $n = 0, \pm 1$ will be ignored for the present to focus attention on the small-signal properties of Fig. 3.

2.2 Solution When $V_n = 0$, $|n| > 1$

Using the approximate value for B_n given in (11b), (10) yields:

$$\frac{V_1}{V_o} = \frac{-jrQ(1 + z)}{2(1 + 2jzQ)} \tag{16a}$$

$$\frac{V_{-1}}{V_o} = \frac{-jr^*Q(1 - z)}{2(1 - 2jzQ)} \tag{16b}$$

$$\frac{I_{oc}}{V_o} = G\left[1 + \frac{|r|^2Q^2}{2}\left(\frac{1 - 2jz^2Q}{1 + 4z^2Q^2}\right)\right] \tag{16c}$$

where $z = \omega_s/\omega_o$, and $r = C_s/C$. An interesting feature revealed by (16) is that the two sidebands have unequal amplitudes, these being in proportion to their respective frequencies:

$$\left| \frac{V_1}{V_{-1}} \right| = \frac{1 + z}{1 - z} \tag{17}$$

One might be tempted to attribute this result to the approximations made in ignoring higher-order sidebands, but (11) is a true limiting value independent of both r and Q. Further inspection of (12) reveals that sideband asymmetry is a general characteristic of this circuit, since it continues to occur as additional sideband pairs are introduced. The significance of this asymmetry will now be demonstrated.

By neglecting all but the first-order sidebands in (4), the total tank voltage in Fig. 3 becomes

$$v(t) = \mathrm{Re} \left\{ V_o e^{jx} \left[1 + \frac{V_1}{V_o} e^{jy} + \frac{V_{-1}}{V_o} e^{-jy} \right] \right\} \tag{18}$$

Since the origin of time in (18) is arbitrary, it will be convenient to choose the phase of r equal to $\tan^{-1} 2zQ$, which simplifies (16). Equation 18 now becomes

$$v(t) = \overline{V}_o \left\{ (1 + 2zS \sin y)^2 + (2S \cos y)^2 \right\}^{\frac{1}{2}} \cos \left[x + \varphi(t) + \varphi_o \right] \tag{19a}$$

where:

$$\varphi(t) = \tan^{-1} \frac{2S \cos y}{1 + 2zS \sin y} \tag{19b}$$

$$V_o = \overline{V}_o e^{j\varphi_o} \tag{20a}$$

$$S = \left| \frac{rQ}{2(1 + 2jzQ)} \right| \tag{20b}$$

The effect of sideband asymmetry is now revealed through terms in (19a) containing the frequency ratio z, since these terms would not occur in

the typical phasor description of angle modulation, such as that used to obtain (2). In (19a) and (19b), the term 2zS sin y contributes to both phase and amplitude distortion. Although both of these effects are very small under the present assumptions, it is instructive to inquire about their origin. The total power delivered by the two sidebands is

$$P_{sb} = \frac{1}{2}(|V_1|^2 + |V_{-1}|^2)\, G$$

$$= S^2 \bar{V}_o^{\,2} (1 + z^2)\, G \qquad (21)$$

The total power supplied to the sidebands by $i_o(t)$ is (by Eq. 16c)

$$G\, S^2 \bar{V}_o^{\,2} \qquad (22)$$

So the power supplied by the time-varying capacitor must be the difference between (22) and (21), or

$$P_s = S^2 \bar{V}_o^{\,2}\, z^2\, G \qquad (23)$$

which increases proportionally to the square of the signal frequency. Therefore, the sideband asymmetry noted in (17) must be due to the energy contribution from the time-varying capacitor $c_s(t)$. The power gain between this time-varying capacitor and the sidebands is

$$\frac{P_{sb}}{P_s} = \frac{1 + z^2}{z^2} = \left(\frac{\omega_o}{\omega_1}\right)^2 \left(1 + \frac{\omega_1}{\omega_o}\right)^2 \approx \left(\frac{\omega_o}{\omega_1}\right)^2 \qquad (24)$$

which is consistent with the fundamental power relations of Manley and Rowe (Ref. 1). Now, if the sideband power in (21) could be completely converted back to f_s, (24) would constitute an overall amplifier power gain, which stresses the importance of this relation.

2.3 Phase Detection

Since the sideband power in (21) is associated with a signal that is essentially phase-modulated, the question arises as to methods of suitable sideband power detection. Rather than employing a typical discriminator circuit, which inherently suppresses the lower video frequencies, direct phase detection appears to be the most efficient approach. Conventionally, the first step in direct phase detection is to add a quadrature carrier component (the pump component in this case) to the phase-modulated signal, which tends to convert the original phase modulation to a proportional amplitude modulation. The second step is envelope detection to recover the original phase information. To demonstrate this principle, (19a) will be rewritten as

$$v(t) = \overline{V}_o \left[1 + A(t)\right] \cos \left[x + \varphi(t) + \varphi_o\right] , \tag{25}$$

and the signal

$$B \sin (x + \theta) \tag{26}$$

will be added to (25) to produce the sum

$$M(t) \cos \left[\omega_o t + \psi(t)\right]$$

where

$$M^2(t) = V_o^2\left[1 + A(t)\right]^2 + B^2 + 2B\, V_o\left[1 + A(t)\right] \sin \left[\theta - \varphi(t)\right] \tag{28a}$$

$$\psi(t) = \tan^{-1}\left\{\frac{\overline{V}_o \left(1 + A(t)\right) \sin (\varphi(t) + \varphi_o) - B \cos \theta}{\overline{V}_o \left(1 + A(t)\right) \cos (\varphi(t) + \varphi_o) + B \sin \theta}\right\} \tag{28b}$$

The phase modulation $\varphi(t)$ now appears on the amplitude envelope. For the case under consideration, where the maximum value of $|\varphi(t)|$ is small, the original amplitude modulation, A(t), is negligible and $\varphi(t)$ makes its greatest contribution to (28a) if $(\theta - \varphi_o) = 0, \pi, \ldots$ In this case, (28a) reduces to

$$M^2(t) \approx \bar{V}_o^2 + B^2 \pm 2 B \bar{V}_o \varphi(t) \tag{29a}$$

$$= (\bar{V}_o^2 + B^2)\left(1 \pm \frac{2 B \bar{V}_o \varphi(t)}{\bar{V}_o^2 + B^2}\right) \tag{29b}$$

But since $|\varphi(t)| \ll 1$

$$M(t) \approx \sqrt{\bar{V}_o^2 + B^2}\left[1 \pm \frac{B V_o \varphi(t)}{\bar{V}_o^2 + B^2}\right] \tag{30}$$

and the resulting envelope waveform approximates

$$\frac{B \bar{V}_o \varphi(t)}{\sqrt{\bar{V}_o^2 + B^2}} \tag{31}$$

which approaches $\bar{V}_o \varphi(t)$ for large B. If $B = \bar{V}_o$, this envelope waveform becomes $0.707 \bar{V}_o \varphi(t)$. For small phase deviations (19b) yields

$$\varphi(t) \approx 2S \cos y \tag{32}$$

so the available power from, say, the positive envelope is

$$\frac{S^2 \bar{V}_o^2 B^2 G}{\bar{V}_o^2 + B^2} \tag{33}$$

while the total sideband power is given by (21). Therefore the fraction of sideband power converted to envelope power, through the addition of a quadrature signal to the original phase modulated signal, is approximately

$$\frac{B^2}{(\bar{V}_o^2 + B^2)(1 + z^2)} \tag{34}$$

which approaches unity for large B and small z. When coupling losses are included with (34), the fraction of sideband power actually available for envelope detection is obtained. This fraction will be referred to as the modulation conversion efficiency. The latter must then be multiplied by the envelope detection efficiency to obtain the total sideband to signal demodulation efficiency.

Returning now to Fig. 2, it can be anticipated that the signal returning to port 3 will contain angle modulation. If so, this modulation can be efficiently detected by positioning the short on arm 4 to reflect a quadrature pump signal back into the junction, where it will add to the signal from arm 3. This sum will then pass through an envelope detector on arm 2. Thus, the basic role of the hybrid junction is to provide conversion from angle to amplitude modulation.

For a symmetrical hybrid, the carriers on arms 3 and 4 are equal (i.e., $B = \bar{V}_o$) so (34) assumes the value one-half. However, another one-half factor must be introduced because half the sideband power incident on the hybrid from arm 3 goes out arm 1. Therefore, the modulation conversion efficiency of the hybrid junction system in Fig. 2 is approximately 25 percent (-6 db). To this must eventually be added the envelope detection loss to arrive at the total demodulation efficiency.

A modification of the hybrid junction phase detector that would avoid much of this 6 db modulation conversion loss is shown in Fig. 4. Assume for illustration that the pump source is increased by 3 db so a -6 db directional coupler will couple out a signal at the original pump level (recall that a hybrid junction acts as a -3db coupler). This

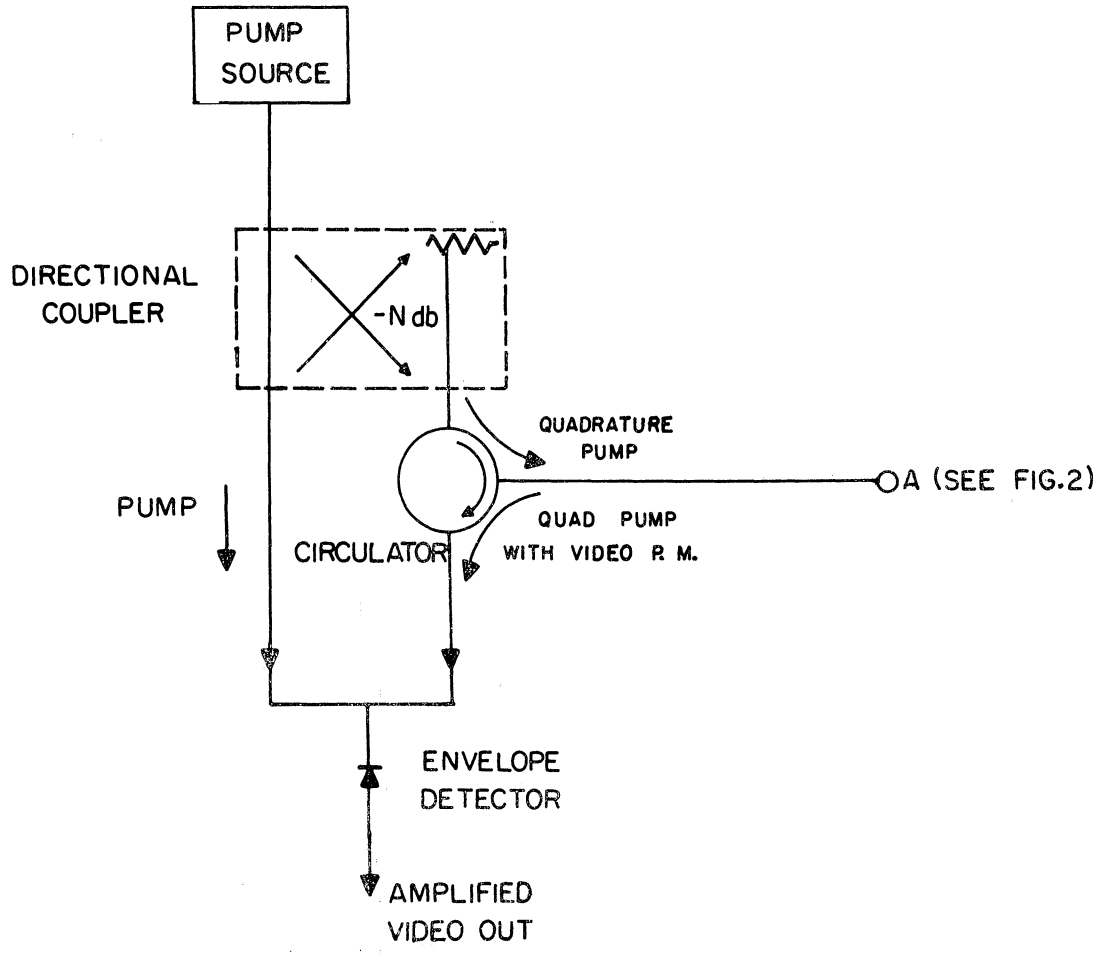

Fig. 4. Modified phase detector to replace hybrid junction in Fig. 2.

signal passes directly into the phase modulator through a circulator, which then channels the entire reflected wave into the envelope detector. The pump source is also applied directly to the envelope detector, so ideally B^2 now exceeds $\bar{V}_o^2$ by 6 db in (34), and (34) becomes approximately -1 db. With this technique, the circulator eliminates the original 3 db insertion loss of the hybrid, and the directional coupler eliminates 2 db of the loss predicted by (34), but requires 3 db more pump power. The directional coupler provides an additional advantage of a $\pi/2$ phase shift,

so the two pump components will arrive at the envelope detector in quadrature, if the line lengths are equal.

3. A MORE GENERAL FORMULATION FOR ANALYSIS OF FIG. 2

The following question arises in attempting to apply the analysis of the previous section to Fig. 2, "Is it valid to neglect nonlinear effects introduced by the large pump signal and then to assume that the varactor follows a small video signal?" To investigate this question, the general behavior of the varactor in Fig. 2 will be considered briefly. Because the varactor capacitance depends upon its terminal voltage, application of the pump (f_o) and the video signal (f_s) will tend to produce pump harmonics (mf_o), video harmonics (nf_s), and mixing products $mf_o \pm nf_s$, where m and n are integers. If low-noise, low-level amplification is of interest, only small video signals need be considered and video harmonics should be of negligible importance. Similarly, pump harmonics can be assumed to be suppressed if the varactor is tuned to the pump frequency, so the major voltage components experienced by the varactor will be at f_o, f_s, and $f_n = f_o + nf_s$, for those values of n that correspond to sidebands within the pump circuit pass band (Fig. 5).

To determine the validity of the assumptions just stated, and of the previous representation of the varactor as a time-varying capacitance at f_s, the following procedure will be carried out with the aid of Fig. 6.

(1) The analysis of Section 2 will be assumed to accurately represent the circuit in Fig. 2. Consequently, all sidebands except those at $f_{\pm 1}$ will be neglected by temporarily assuming them to be short circuited, as shown in Fig. 6a.

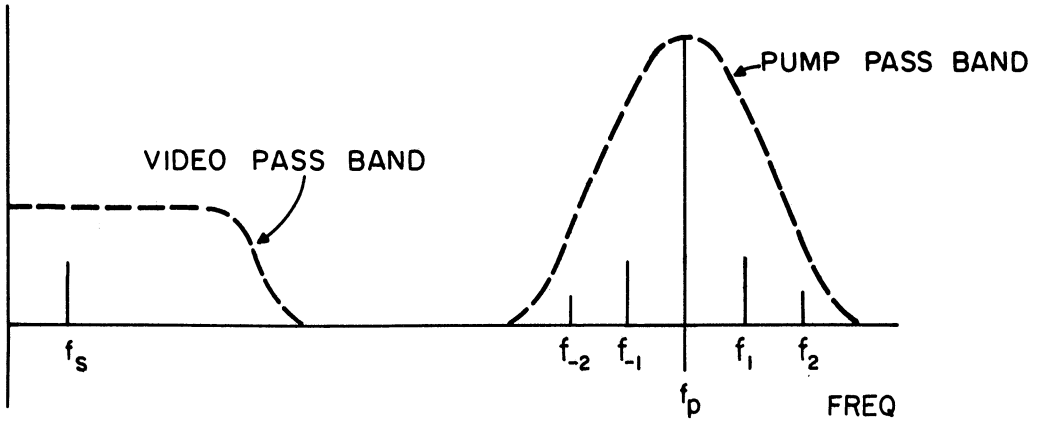

Fig. 5. Anticipated spectral distribution for circuit in Fig. 2, with small video signals.

(2) The total varactor voltage waveform in Fig. 6a will be denoted by

$$V(t) = \overline{V} + v(t) \tag{36a}$$

where $\overline{V}$ is the dc bias voltage and

$$v(t) = \mathrm{Re}\left[V_s e^{jy} + V_o e^{jx} + V_1 e^{j(x+y)} + V_{-1} e^{j(x-y)}\right] \tag{36b}$$

The varactor current, $i(t)$, will have components at the same frequencies as $v(t)$, and short-circuited components $i_{sc}(t)$ in addition. Therefore,

$$i(t) = i_{sc}(t) + \mathrm{Re}\left[I_s e^{jy} + I_o e^{jx} + I_1 e^{j(x+y)} + I_{-1} e^{j(x-y)}\right] \tag{37}$$

(3) The total varactor capacitance, $C_T(V)$, which is defined as the ratio of its total instantaneous charge, $Q(V)$, to total instantaneous voltage, $V(t)$, will be represented by the curve in Fig. 6b. The varactor will be assumed to be biased at a value $\overline{C}$ by the dc voltage $\overline{V}$, and its characteristic in the vicinity of $\overline{C}$ will be represented by

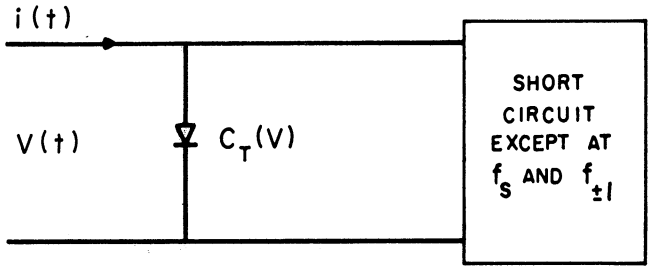

(a)

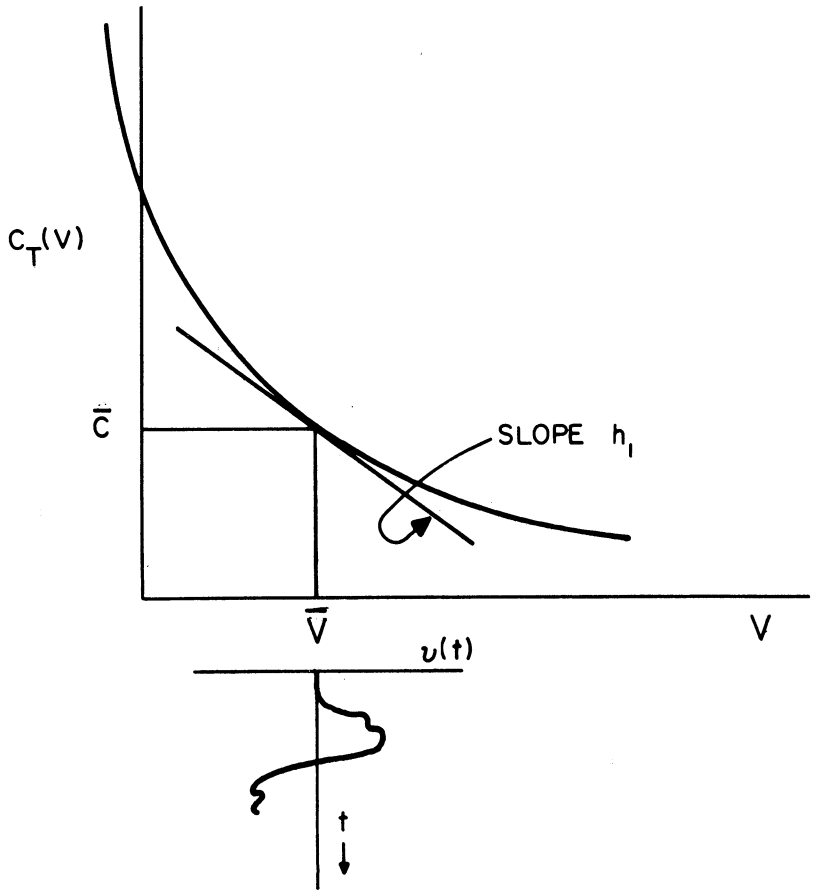

(b)

Fig. 6. Assumed characteristic for total varactor capacitance vs. voltage. $\bar{V}$ is bias voltage.

$$C_T(V) = \bar{C} + h_1 (V-\bar{V}) + \frac{1}{2} h_2 (V-\bar{V})^2 \tag{38}$$

(4) By using this varactor characteristic and the fundamental relation in (6c), basic equations will be derived relating $v(t)$ and the unshorted components of $i(t)$. These equations will be shown to be consistent with those derived in Section 2, and will be used to further evaluate the circuit properties of the Brett amplifier. Also, they will be used to derive the components of short-circuit current that were introduced in step (1). Conditions will then be obtained to show when the short circuits in Fig. 6a can be removed without seriously changing $i(t)$ and $v(t)$.

To proceed with these steps, the instantaneous capacitance of the varactor will be approximated by

$$C_T(t) = \bar{C} + h_1 v(t) + \frac{1}{2} h_2 v^2(t) \tag{39}$$

Although this relation only approximately represents a varactor, it is sufficiently accurate to illustrate the basic mixing process that occurs in Fig. 2. Using this approximation, the basic law for varactor current, in (6c), becomes

$$i(t) = \frac{d}{dt}\left[\left[\bar{C} + h_1 v(t) + \frac{1}{2} h_2 v^2(t)\right]\left[\bar{V} + v(t)\right]\right] \tag{40}$$

Now, substituting (36b) in (40), and comparing the result with (37), yields the following set of fundamental relations:

$$I_s = j\omega_s\left[\eta_1 V_s + \frac{1}{2}\eta_2 V_o^* V_1 + \frac{1}{2}\eta_2 V_o V_{-1}^*\right] \tag{41a}$$

$$I_{-1}^* = -j\omega_{-1}\left[\eta_1 V_{-1}^* + \frac{1}{2}\eta_2 V_o^* V_s\right] \tag{41b}$$

$$I_1 = j\omega_1 \left[\eta_1 V_1 + \frac{1}{2} \eta_2 V_o V_s \right] \tag{41c}$$

$$I_o = j\omega_o \left[\eta_1 V_o + \frac{1}{2} \eta_2 V_1 V_s^* + \frac{1}{2} \eta_2 V_{-1} V_s \right] \tag{41d}$$

where:

$$\eta_1 = \overline{C} + h_1 \overline{V} \; ; \qquad \eta_2 = 2h_1 + h_2 \overline{V} \tag{41e}$$

These equations describe a mixing process that can be traced through, starting with I_s and I_o. The first terms in (41a) and (41d) show that I_s and I_o experience an effective varactor capacitance equal to η_1, which gives rise to voltage components V_s and V_o. In turn, these voltages produce sideband currents through the mixing terms $\frac{1}{2} \eta_2 V_o^* V_s$ in (41b) and $\frac{1}{2} \eta_2 V_o V_s$ in (41c). These sideband currents also experience the effective varactor capacitance η_1, producing sideband voltages that mix to produce reflected currents at f_s and f_o, according to the last two terms in (41a) and (41d).

Equations (41) demonstrate that η_1 is the effective varactor capacitance, since this value of capacitance is experienced when a (small) sinusoidal signal, plus bias, is applied to a varactor (i.e., when V_s and $V_{\pm 1}$ are zero). Therefore, published curves of varactor capacity vs. bias, that are measured by RF techniques, are actually plots of η_1 and have slope η_2.

It is instructive to note that the set (41) would also be obtained if the varactor were represented by the following charge-voltage characteristic:

$$Q(V) = \overline{C}\,\overline{V} + \eta_1 (V - \overline{V}) + \frac{1}{2} \eta_2 (V - \overline{V})^2 \tag{42}$$

Again, η_1 and η_2 are related to the coefficients in (38) by (41e).

The relations in (41) can now be used to answer the question posed at the beginning of this section, which asked if it was valid to assume that the varactor follows only one of two applied signals, as in Fig. 2. This question will be answered by showing that the set of non-linear equations in (41) can be solved by converting it to one of two linear sets; each of which applies when the varactor follows only one signal, either the signal at f_s or the signal at f_o. Therefore, these two cases result from replacing the varactor by a time-varying capacitor at either f_s or f_o. It will be shown below that these two representations are related by the symmetry that occurs with respect to V_o (or V_o^*) and V_s in the mixing terms in (41b) and (41c).

3.1 Formulation for a Time-Varying Capacitor at f_s

This representation arises because (41b) through (41d) can also be derived from (6c) if, before substituting in (6c), V_s is deleted from (36b), and (39) is replaced by the following harmonically-varying capacitance

$$\eta_1 + c_s(t) = \eta_1 + \eta_2 \mathrm{Re}\left[V_s e^{j\omega_s t}\right]$$

Physically this situation is identical to that treated in Section 2, and it can be made mathematically equivalent by letting

$$C = \eta_1 + \text{stray capacity} \tag{43a}$$

$$C_s = \eta_2 V_s \tag{43b}$$

This equivalence is seen by comparing (41b) through (41d) with (8) or (10). The significance of (43b) is consistent with intuition, since it shows that $C_T(t)$ follows the video voltage, in proportion to the slope (η_2) of

the effective capacitance characteristic. Now, since (43) converts (41b) through (41d) into a linear set whose solution was given in Section 2, this solution can now be substituted into (41a) to relate C_s (or V_s) to the video current I_s, which completes the solution of the set (41). However, the actual implementation of this step will be postponed until Section 4.

3.2 Formulation for a Time-Varying Capacitance at f_o

This representation arises in a similar manner to the previous one, although it is derived from the first three equations of (41), instead of the last three. If $C_T(t)$, in (39), is replaced by the following harmonically-varying capacitance (at f_o)

$$\eta_1 + \mathbf{c}_o(t) = \eta_1 + \eta_2 \, \mathbf{Re}\left[V_o e^{j\omega_o t} \right] \tag{44a}$$

and if V_o is deleted from (36b), then (6c) will again yield (41a) through (41c) if

$$C_o = \eta_2 V_o \tag{44b}$$

The latter relation now converts (41a) through (41c) into a linear set, whose solution can be substituted into (41d) to again complete the solution of the set (41).

3.3 Summary of Section 3

It can now be concluded, within the assumptions stated at the start of this section, that the varactor in Fig. 2 can be considered to follow either the small video signal or the large pump signal, since these approaches lead to the same solution for the set (41). This property is the result of the symmetry of the mixing terms in (41b) and (41c), which

can be illustrated as follows. Note that mixing occurs in (41b) through the term $\eta_2 V_o^* V_s$, but this term can be treated equally well as: (1) a capacitor $\eta_2 V_s$ mixing with V_o^*, or (2) as a capacitor $\eta_2 V_o^*$ mixing with V_s; and either case leads to a systematic solution of (41).

The final step of verifying the assumptions at the beginning of this section is mainly of mathematical interest, so it is treated in Appendix 1. Since Appendix 1 makes use of relations that are derived in Section 4, it should be noted for now that the above procedure is valid if $|V_s| \ll |V_o|$.

4. CIRCUIT PROPERTIES OF THE BRETT PARAMETRIC VIDEO AMPLIFIER

Through the introduction of (41a), the analysis in Section 3 has provided a method for using the results of Section 2 to determine more of the properties of Fig. 2. However, the alternate approach outlined in Section 3.2 is more conventionally used for deriving the properties of reactive mixer circuits (Refs. 2 and 4). Therefore, for ease of comparison with other works in this area, the method of replacing the varactor by the time-varying capacitor in (44a) will be used to relate (41) to Fig. 2 and to thereby obtain the basic properties of this circuit. At the same time, the effective varactor capacitance η_1 will be denoted by C to be consistent with Fig. 3.

To go to this second analysis, a more precise specification of the circuit in Fig. 2 is necessary. The analysis of the previous section employed lumped circuit concepts, and therefore the circuit in Fig. 7 provides a useful equivalent for that in Fig. 2. In Fig. 7, a hybrid coil has been substituted for the hybrid junction, and simple filters separate the video and pump signals that appear across the

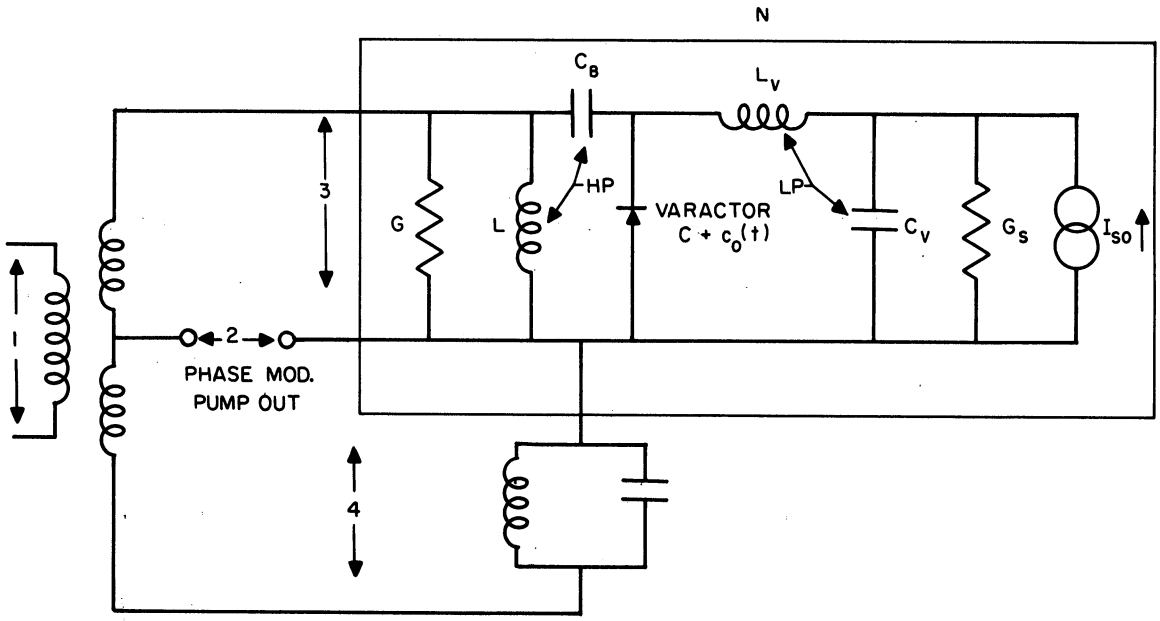

Fig. 7. A lumped parameter equivalent circuit for Fig. 2. $L_B \gg L$ and $C_B \gg C$ are assumed.

varactor. The tuned circuit on arm 4 represents the adjustable short in the transmission line version (Fig. 2). It will be recalled that this short provides a variable pump component that can be added to the phase-modulated signal on arm 3 to accomplish phase detection.

At video frequencies, I_{so} is the video source, and the varactor network N in Fig. 7 reduces to Fig. 8a. At the sideband frequencies ($f_{\pm 1}$) N reduces to Fig. 8b (Note: the sideband current sources that have been included in Fig. 8b will be treated as noise generators in Section 5.3 so they will be carried along in the present analysis.)

By Figs. 8a and 8b,

$$I_{so} = I_s + (G_s + j\omega_s[C + C_V + C_B])\, V_s = I_s + Y_s V_s \qquad (45a)$$

$$I_{1O} = I_1 + Y_1 V_1 \; ; \; I_{-1O} = I_{-1} + Y_{-1} V_{-1} \qquad (45b)$$

where Y_1 and Y_{-1} are defined in (11a) and (11b) and are again assumed to

have the value

$$Y^*_{-1} = Y_1 \approx G + 2j\omega_s C \ . \tag{46}$$

Note: This assumed symmetry of the pump circuit admittance will be shown to have an important bearing on the operation of the Brett circuit.

Now, by combining (41a) through (41c) with (45), the following fundamental admittance relation is obtained (Refs. 2 and 4).

$$\begin{vmatrix} I_{so} \\ I_{1o} \\ I^*_{-1o} \end{vmatrix} = \begin{vmatrix} Y_s & \frac{1}{2} j\omega_s C^*_o & \frac{1}{2} j\omega_s C_o \\ \frac{1}{2} j(\omega_1) C_o & Y_1 & 0 \\ -\frac{1}{2} j(\omega_{-1}) C^*_o & 0 & Y^*_{-1} \end{vmatrix} \begin{vmatrix} V_s \\ V_1 \\ V^*_{-1} \end{vmatrix} \tag{47}$$

Since the approximation cited in (46) will be assumed in applying (47), Y^*_{-1} can be replaced by Y_1. It should be noted that (47) plays the same role as (12) did in Section 2, and therefore it will yield the basic circuit properties of Fig. 7, which are given in the following sections (see Refs. 2 and 4 for typical derivations of these quantities). It should also be noted that the procedure outlined in Section 3.1 leads to identical circuit properties.

4.1 Total Input Admittances Presented to the Ideal Sources In Figs. 8a and 8b.

$$\underline{\text{At } \omega_s :} \qquad Y_{s_{IN}} = Y_s + \frac{\omega_s^2 |C_o|^2}{2Y_1} \tag{48a}$$

$$\underline{\text{At } \omega_1 :} \qquad Y_{1_{IN}} = Y_1 + \frac{\omega_s \omega_1 |C_o|^2 Y_1}{4 Y_s Y_1 - \omega_s \omega_{-1} |C_o|^2} \tag{48b}$$

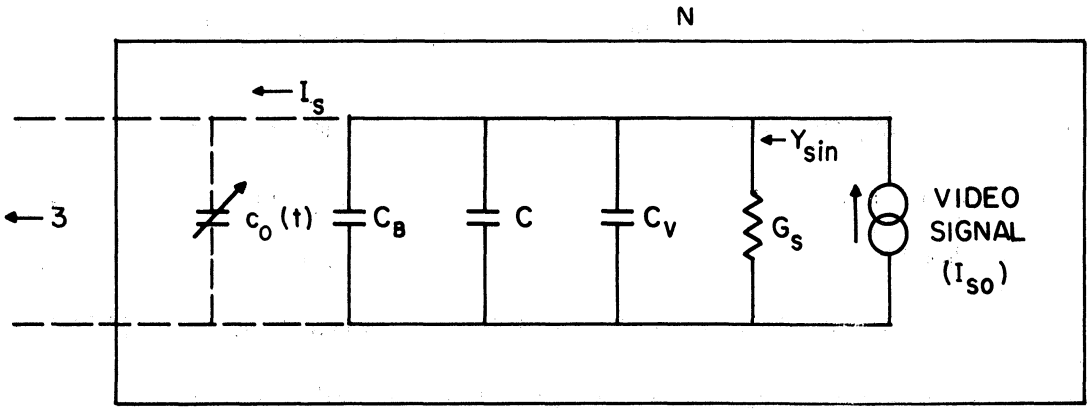

Fig. 8(a). Video equivalent of N in Fig. 7.

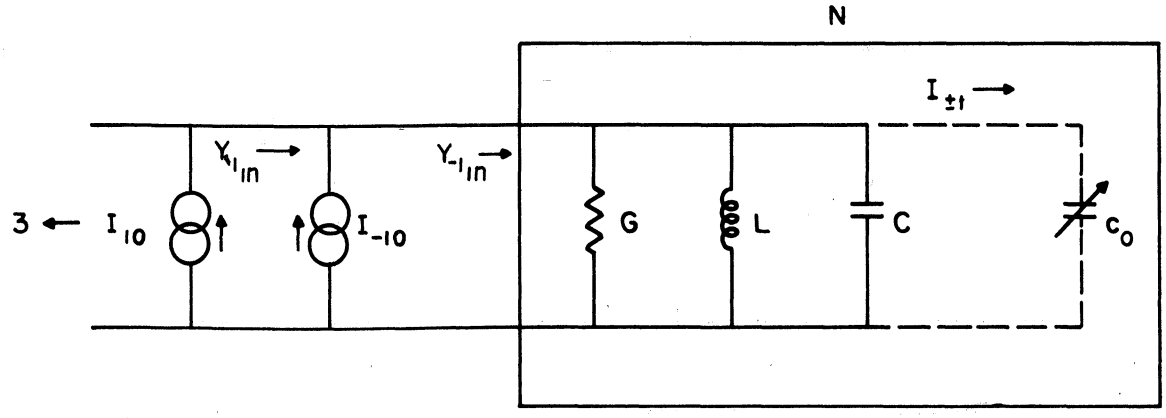

Fig. 8(b). High frequency equivalent of N in Fig. 7.

$$\underline{\text{At } \omega_{-1}:} \qquad Y_{-1_{IN}} = Y_1^* - \frac{\omega_s \omega_{-1} |C_o|^2 Y_1^*}{4\, Y_s^* Y_1^* + \omega_s \omega_1 |C_o|^2} \tag{48c}$$

Perhaps one surprising result in (48a) is that the reflected input admittance at ω_s (the second term in 48a) has a positive real part. The derivation of (48a) shows that this result is a consequence of the slight difference between the amplitudes of V_1 and V_{-1}, as first noted in (17). This difference arises in spite of the pass band symmetry assumed in (46). A second feature of (48) to be noted is that $Y_{1_{IN}} \neq Y_{-1_{IN}}$ even though $Y_1 = Y_{-1}^*$. This result has bearing on the overall circuit-noise figure.

4.2 Transducer Gain Between ω_s and $\omega_{\pm 1}$

The transducer gain $(TG)_{sn}$ from ω_s to ω_n is defined as the output power at ω_n divided by the available source power at ω_s. By (47),

$$\underline{\omega_s \rightarrow \omega_1:} \qquad (TG)_{s1} = \frac{G_s G\, \omega_1^2 |C_o|^2}{|Y_s Y_1 + \frac{1}{2}\omega_s^2 |C_o|^2|^2} \tag{49a}$$

$$\underline{\omega_s \rightarrow \omega_{-1}:} \qquad (TG)_{s,-1} = \frac{G_s G\, \omega_{-1}^2 |C_o| C_o|^2}{|Y_s Y_1 + \frac{1}{2}\omega_s^2 |C_o|^2|^2} \tag{49b}$$

4.3 Gain-Bandwidth Products for Conversion Between ω_s and $\omega_{\pm 1}$

Because V_1 and V_{-1} combine with the pump to produce an angle modulated signal, the total power in V_1 and V_{-1} will eventually determine the video power available from the final envelope detector. Therefore, the sum of the two transducer gains in (49) is of basic interest, namely

$$\begin{aligned} (TG)_s &= (TG)_{s1} + (TG)_{s,-1} \\ &= \frac{G G_s\, (\omega_o^2 + \omega_s^2) |C_o|^2}{|Y_s Y_1 + \frac{1}{2}\omega_s^2 |C_o|^2|^2} \end{aligned} \tag{50}$$

which will be considered a function of ω_s. In evaluating (45) and other related quantities, it will be convenient to introduce the following auxiliary parameters:

$$\rho_s = \frac{G_s}{C + C_v + C_B} = \text{video circuit bandwidth (radians)} \tag{51a}$$

$$\rho_o = \frac{G}{2C} = \text{one-half pump circuit bandwidth (radians)} \tag{51b}$$

$$\alpha = \frac{|C_o|^2}{4C(C + C_v + C_B)} \tag{51c}$$

Equation (50) now becomes

$$(TG)_s = \frac{4\alpha\left(\frac{\omega_o}{\rho_s}\right)\left(\frac{\omega_o}{\rho_o}\right)\cdot\left(1 + \frac{\omega_s^2}{\omega_p^2}\right)}{\left|1 + (\alpha-1)\left(\frac{\omega_s^2}{\rho_s\rho_o}\right) + j\omega_s\left(\frac{1}{\rho_o} + \frac{1}{\rho_s}\right)\right|^2} \tag{52}$$

Therefore, maximum gain occurs at $\omega_s = 0$ and has the value

$$(TG)_0 = \frac{4\alpha\,\omega_o^2}{\rho_s\rho_o} \tag{53}$$

The bandwidth ρ of $(TG)_s$ is also of interest, and to calculate this quantity it will be assumed that $\omega_s \ll \omega_p$ at the -3 db points. In this case

$$\rho = \sqrt{\rho_o\rho_s}\left[\frac{-|K| + \sqrt{|K|^2 + 1}}{1-\alpha}\right]^{\frac{1}{2}} \tag{54a}$$

where

$$|K| = \frac{1}{2(1-\alpha)}\left(\sqrt{\frac{\rho_s}{\rho_o}} + \sqrt{\frac{\rho_o}{\rho_s}}\right)^2 - 1 \tag{54b}$$

$$\alpha \leq 1$$

Inspection of these relations shows that ρ can be approximated by

$$\boxed{\rho \approx \left(\frac{1}{\rho_s} + \frac{1}{\rho_o}\right)^{-1}} \tag{55}$$

This approximation is very accurate for

$$\frac{\beta_s}{\beta_o} \ll 1, \qquad \text{or} \qquad \frac{\beta_s}{\beta_o} \gg 1$$

and incurs a maximum error of about 30 percent for $\beta_s = \beta_o$ and $\alpha \approx 0$. Exact solutions of (54a) and (54b) are plotted in Fig. 9 for $\alpha = 0$ and $\alpha = 1$. For other values of α, the curves for β lie between those plotted; so (55), which corresponds to the $\alpha = 1$ curve in Fig. 9, can be taken as a practical lower bound on the bandwidth of $(TG)_s$.

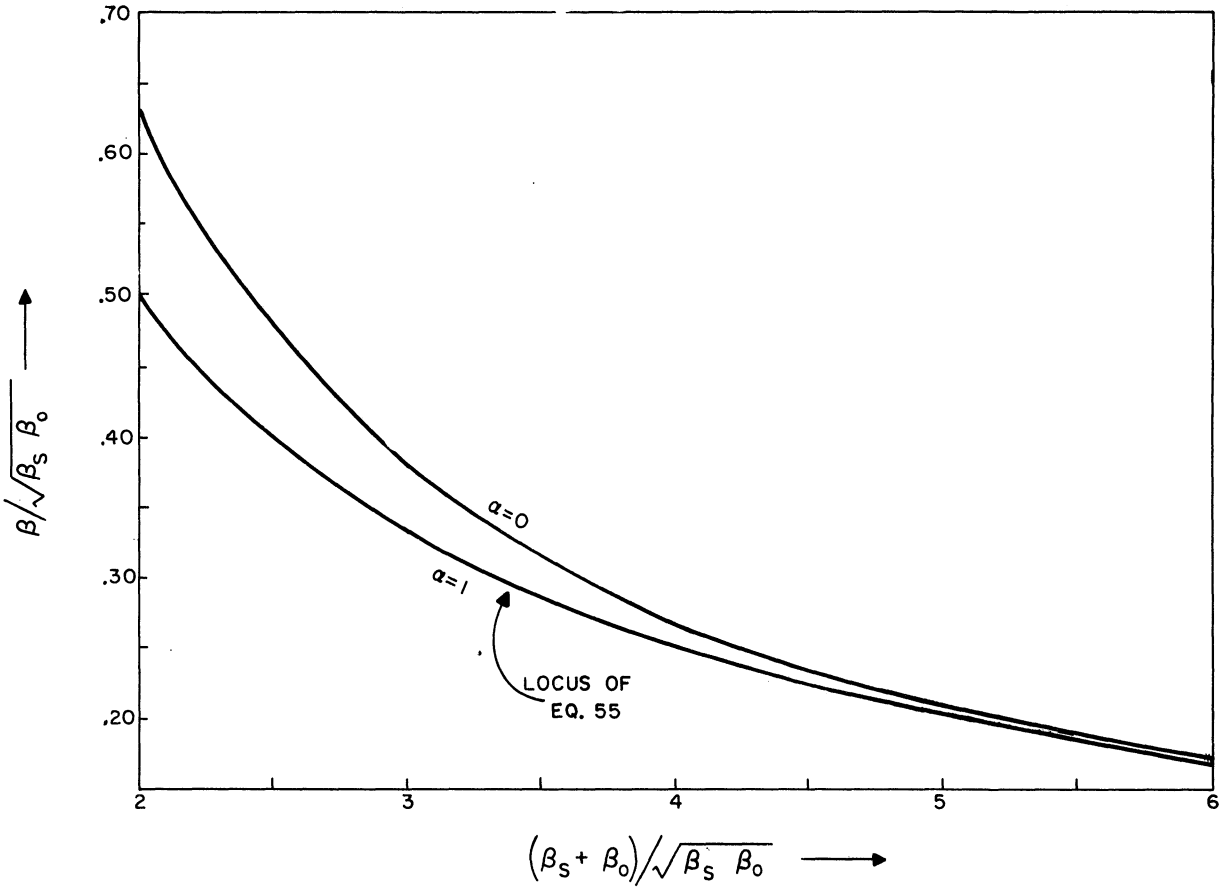

Fig. 9. Upper and lower bounds on conversion bandwidth vs. the sum of the circuit bandwidths, normalized to $\sqrt{\beta_s\,\beta_p}$.

Now, combining (53) with (55) yields the following lower bound for the gain-bandwidth product of the circuit in Fig. 7.

$$(GB) = \frac{\beta \sqrt{(TG)_o}}{2\pi} \geq \frac{\omega_p}{\pi} \sqrt{\frac{\alpha}{\frac{\beta_s}{\beta_o} + \frac{\beta_o}{\beta_s}}} \tag{56}$$

The expression on the right has a maximum value when $\beta_s = \beta_o$, or

$$(GB)_{MAX} \geq f_p \sqrt{2\alpha} \tag{57}$$

which emphasizes the value of a high pump frequency.

4.4 Numerical Example

Because of the abundance of circuit variables introduced thus far, a numerical example will perhaps be appreciated. Assume that a video amplifier is to be designed with the following characteristics:

Maximum Gain (dc) = 20 db

Bandwidth = 100 Mc

Pump Frequency = 5000 Mc

If $\beta_s = \beta_o$ these requirements yield

$$\text{(by Eq. 57)} \quad \alpha < \left[\frac{(10)(100\text{ Mc})}{\sqrt{2}\ (5000\text{ Mc})}\right]^2 = 0.02$$

$$\text{(by Eq. 55)} \quad \frac{\beta_s}{2\pi} = \frac{\beta_o}{2\pi} = 2\ (100\text{ Mc}) = 200\text{ Mc}$$

However, with β_s chosen equal to β_o and α very much less than one, the calculations above contain nearly the full 30 percent error in (55). The exact solution of (54) in this case yields

$$\beta = 0.65\ \beta_s \tag{58a}$$

so (56) becomes

$$(GB) = \frac{\sqrt{2\alpha}}{0.65} f_o \qquad \alpha << 1 \qquad (58b)$$

Hence, the conditions in this example can be more accurately satisfied with

$$\text{(by 58b)} \qquad \alpha = 0.0084$$

$$\text{(by 58a)} \qquad \frac{\beta_s}{2\pi} = \frac{\beta_o}{2\pi} = 154 \text{ Mc}$$

It will be shown later that the value 0.0084 is well within the physical limitations on α.

To complete the example under discussion, when $\beta_s = \beta_o$ the video input admittance can be written

$$Y_{s_{IN}} = \left[1 + \frac{\alpha\left(\frac{\omega_s}{\beta_s}\right)^2}{1 + \left(\frac{\omega_s}{\beta_s}\right)^2} \right] G_s + j \left[\frac{\omega_s}{\beta_s} - \frac{\alpha\left(\frac{\omega_s}{\beta_s}\right)^2}{1 + \left(\frac{\omega_s}{\beta_s}\right)^2} \right] C_s$$

By this relation, it is evident that $Y_{s_{IN}}$ is very nearly equal to Y_s as long as $\alpha << 1$, which means that the circuit in this example operates essentially as a voltage amplifier. The fact that very little video power is accepted at the input terminals also explains the difference between the power gains in (50) and (24). The former depends upon the video power available at the input while the latter depends upon video power delivered to the input.

A final calculation of interest is the total transducer gain, which (by 52) is given very nearly by

$$(TG)_s \approx \frac{100}{\left[1 + \left(\frac{\omega_s}{\beta_o}\right)^2\right]^2}$$

This quantity is plotted in Fig. 10 and shows a 12 db/octave roll off at high frequency and a half-power bandwidth of very nearly 100 Mc.

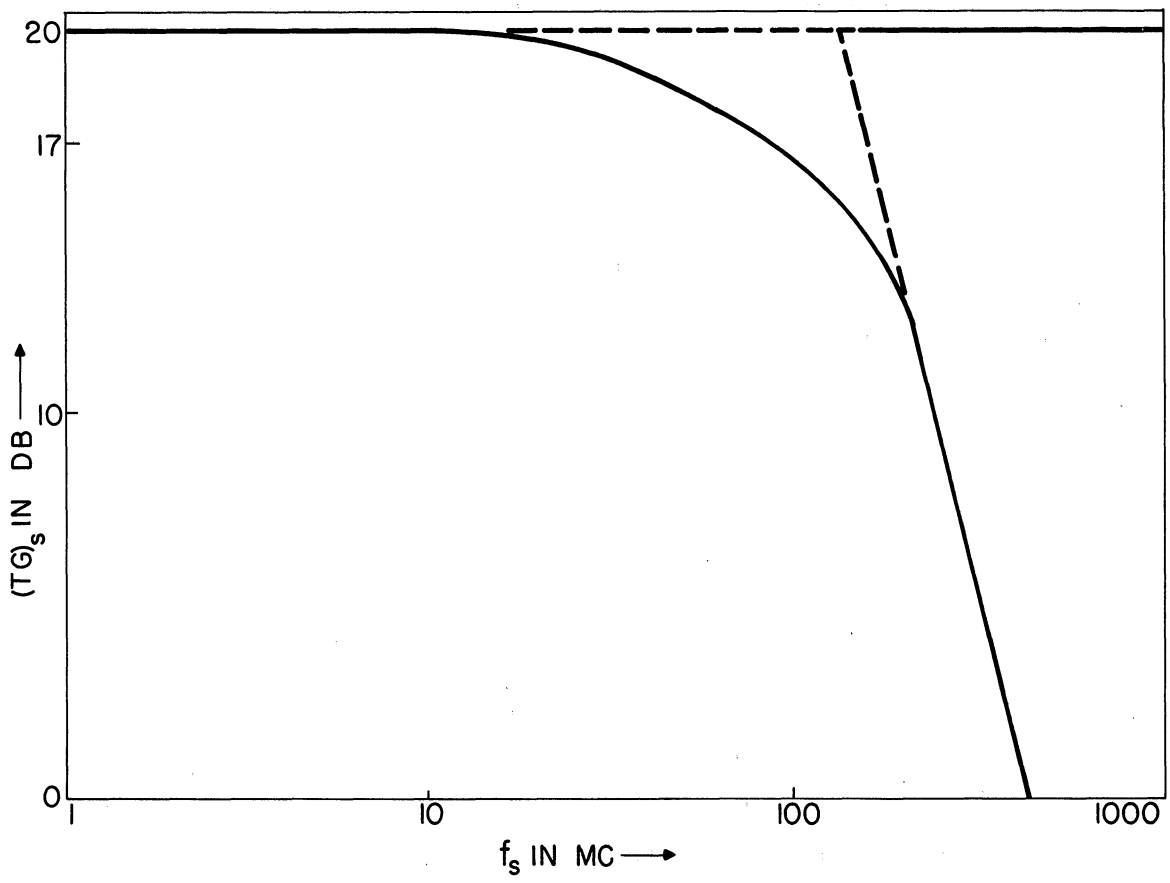

Fig. 10. Gain characteristic of example video parametric amplifier, pump frequency 5000 Mc.

5. DESIGN CONSIDERATIONS FOR OPTIMUM AMPLIFIER PERFORMANCE

5.1 Physical Limitations on α

Since gain-bandwidth product (by 56) is proportional to $\sqrt{\alpha}$, it is important to consider possible limitations on this quantity. By definition (in 51c), α is one-fourth of the ratio of the dynamic varactor capacitance squared (C_o^2) to the product of the total fixed capacitance shunting C_o at f_s and f_o. Thus maximum α occurs when the varactor experiences minimum stray, filter, or bypass capacitance at each operating frequency, or

$$\alpha_{MAX} = \left(\frac{C_o}{2C}\right)^2 \tag{59}$$

and by (44a) and (44b)

$$\alpha_{MAX} \approx \left(\frac{\eta_2 \, \overline{V}_o}{2 \, \eta_1}\right)^2 \tag{60}$$

It should be noted that (60) is strictly valid only for $\overline{V}_o/\overline{V} \ll 1$, or when the effective varactor capacity η_1 can be assumed to vary linearly about its value at $\overline{V}$. However, graphical analysis of typical varactor characteristics will show that (60) does approximate (59) over a significant range of $V_o/\overline{V}$.

It is well known that the charge-voltage characteristic of back biased semiconductor diodes can be approximated by the relation

$$Q(V) = Q' \left(1 + \frac{V}{V_c}\right)^{-m} ; \qquad 0 < m < 1 \tag{61}$$

where V_c is the junction contact potential and normally $V_c \ll \overline{V}$. Therefore, by (42),

$$\eta_1 = \left(\frac{m}{A}\right) Q(\overline{V}) \left(1 + \overline{V}/V_c\right)^{-1}$$

$$\eta_2 = \left(\frac{m-1}{A}\right) N_1 \left(1 + \bar{V}/V_c\right)^{-1}$$

and so (60) becomes

$$\alpha_{MAX} \approx \left(\frac{m-1}{2}\right)^2 \left(\frac{\bar{V}_o}{\bar{V}_c}\right)^2 \left(1 + \bar{V}/V_c\right)^{-1}$$

which reduces to

$$\left(\frac{m-1}{2}\right)^2 \left(\frac{\bar{V}_o}{\bar{V}}\right)^2$$

if $\bar{V}_o$, $\bar{V} \gg \bar{V}_c$. Since $\bar{V}_o = \bar{V}$ marks the threshold of excessive varactor conduction, the upper limit on α that is predicted by (60) will be taken to $\left[(m - 1)/2\right]^2$, which has the value 0.06 for the typical case of $m = 1/2$. However, for $\bar{V}_o \approx \bar{V}$, the accuracy of (60) deteriorates, and an exact Fourier analysis is required to evaluate (59). This has been done in Ref. 6, and the result for $m = 1/2$ is shown in Fig. 11. Since the latter curve predicts $\alpha \approx 0.1$ for $V_o/V = 0.9$, the value 0.1 will be taken as a safe upper limit on α, in the sense that $\alpha = 0.1$ should be approachable with large pump signals and minimum stray or auxiliary capacity across the varactor.

Filter or bypass capacity that may shunt the varactor on one or more of the operating frequencies will reduce both α and the circuit bandwidth, but these reductions will produce opposing effects on the transducer gain (by 52). To illustrate this point, consider a case where the input signal is available from a 100 ohm source and the effective varactor capacitance (C) is 1 pf, so (neglecting any bypass capacity) $\beta_s/2\pi = 1600$ Mc. If the desired amplifier bandwidth is significantly smaller than 1600 Mc, the extra input circuit bandwidth in this case would unnecessarily reduce the transducer gain; but if β_s is reduced by

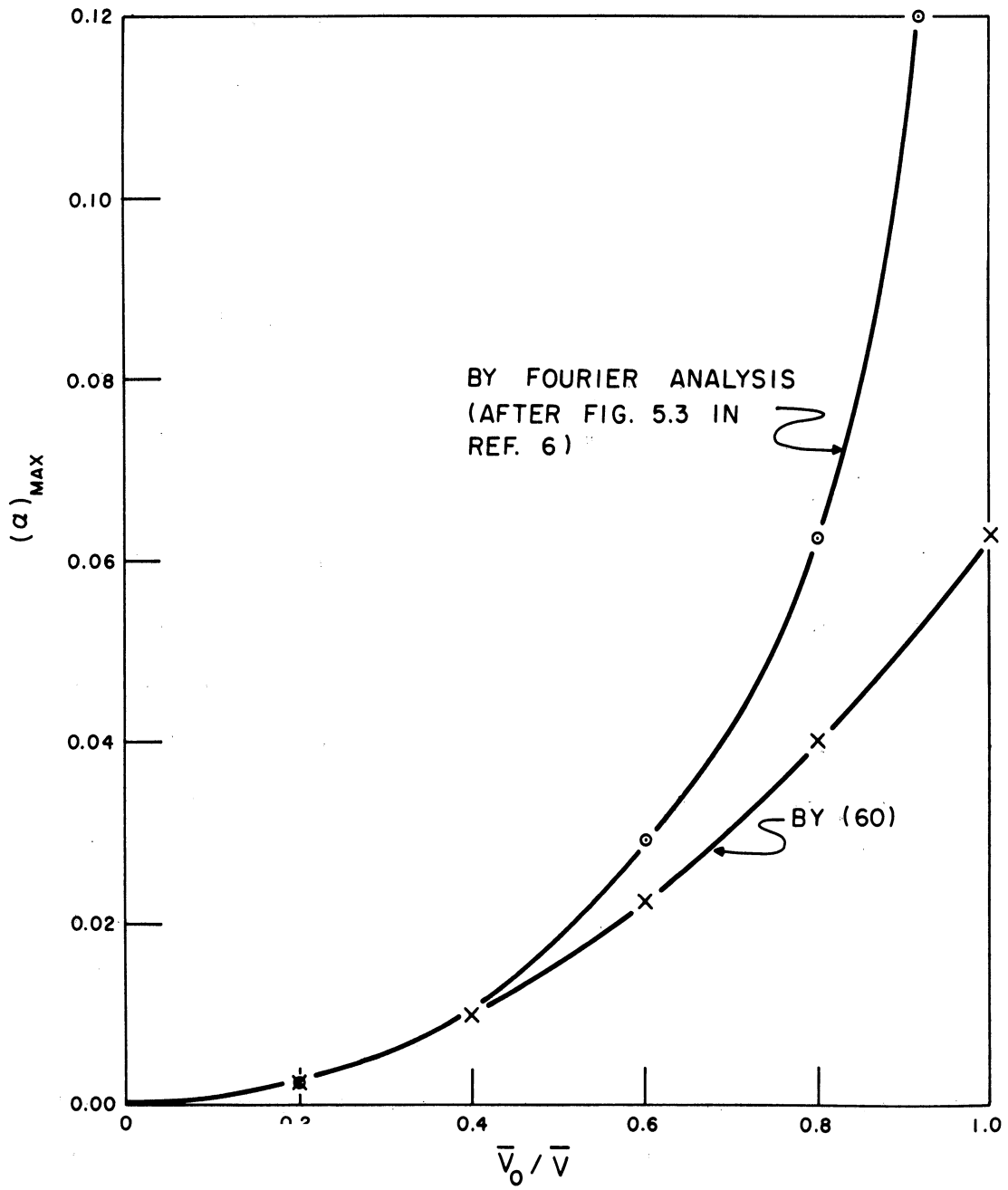

Fig. 11. Estimates of $(\alpha)_{MAX}$.

adding extra capacity in the video circuit, α will be reduced simultaneously to nullify the possible advantage to be derived from the former reduction. Therefore, to make optimum use of the varactor, video bandwidths must be controlled by inductive source transformations.

To continue the illustration above, a stray capacity of 1 pf will be allowed for, making $C + C_s = 2$ pf, and a broadband 2:1 step-up transformer will be assumed to change the source impedance to 400 ohms. Then $\beta_s/2\pi$ is reduced to 200 Mc, with an accompanying transducer gain improvement of 6 db (Note: the reduction in β_s accounts for 9 db, while the reduction in α accounts for -3 db). In the Brett amplifier, the importance of a high source impedance arises because the video input impedance is large as long as $f_s \ll f_o$. Thus, as a wideband amplifier, the Brett circuit is particularly useful with high impedance sources such as solid state particle detectors or various photoelectric devices.

5.2 Operation With State-of-the-Art Limitations on Varactor Elements

The equation for maximum gain bandwidth product (57) suggests that f_o should be as large as possible, but the high frequency losses in actual varactors make this choice incompatible with the other optimizing condition that $\beta_s = \beta_o$. The high frequency loss in a varactor is due to a fairly constant series resistance R, and therefore the varactor will load the pump tank (see Fig. 12) with an effective shunt conductance

$$G_D \approx \omega_o^2 RC^2 = \frac{Q_D^2}{R} = \frac{\omega_o^2 C}{\omega_D} \qquad (62)$$

where Q_D is the Q of the varactor at ω_o, and ω_D is the frequency where $Q_D = 1$ (commonly termed the varactor cut-off frequency). The approximation in (62) is valid if $Q_D^2 \gg 1$.

In Fig. 12, G_L represents the effective shunt conductance of the external circuit, so the total tank conductance G is the sum $G_L + G_D$. Regarding Fig. 2, G_L represents the conductance seen looking into arm 3 of the hybrid junction, which in turn depends upon the internal conductance of the pump generator and the external load conductance reflected through the envelope detector. If these are both matched to the hybrid, G_L will be the characteristic admittance of the hybrid junction. In the case of the modified pump circuit in Fig. 4, the nonreciprocal properties of the circulator cause G_L to depend only upon the envelope detector and its output load. Henceforth, G_L will be assumed to included all external loading on the pump tank, but its precise value will depend upon the particular pump circuit configuration employed.

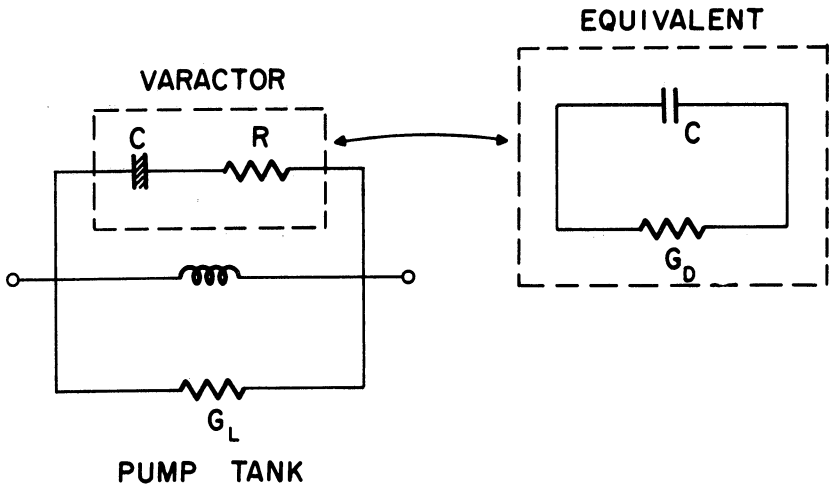

Fig. 12. Pump tank with varactor loss R and external load G_L.

With varactor loss, the half-bandwidth of the pump circuit is

$$\beta_o = \frac{G_D + G_L}{2C} = \beta_D + \beta_L \qquad (63a)$$

where

$$\beta_D = \frac{G_D}{2C} \; ; \; \beta_L = \frac{G_L}{2C} \tag{63b}$$

For a given pump frequency, it is evident that the minimum value of β_o is β_D, which can also be expressed as

$$(\beta_o)_{MIN} = \beta_D = \frac{\omega_o^2}{2\omega_D} \tag{64}$$

Similarly, the expression in (53) for low frequency gain must be changed to account for varactor loss. It will be sufficient to do this by considering the transducer gain between source and G_L rather than G, or

$$(TG)_0 = \frac{4\alpha\omega_o^2}{\beta_s \beta_o} \left(\frac{G_L}{G_L + G_D} \right) \tag{65a}$$

and by (64) and (63b)

$$(TG)_0 = \frac{8\alpha\omega_D}{\beta_s} \left[\frac{\beta_L \beta_D}{(\beta_L + \beta_D)^2} \right] \tag{65b}$$

Since (65b) is maximum for $\beta_L = \beta_D$, varactor loss will be best compensated for by choosing $G_L = G_D$, which yields

$$(TG)_0 = \frac{2\alpha\omega_D}{\beta_s} \tag{66}$$

In practice, (66) must now be reduced by the fraction of G_L that constitutes the actual output load, but this step will not alter the significance of this relation.

From (66), it is now desirable to minimize β_s. By (55) and (63), the bandwidth (β) can be approximated by the relation

$$\frac{1}{\beta} \approx \frac{1}{\beta_s} + \frac{1}{\beta_D + \beta_L}$$

Therefore, if f_o is high enough to make $\beta_D >> \beta_s$, so that $\beta \approx \beta_s$, than the desired amplifier bandwidth will be obtained with maximum gain.

In summary, varactor losses influence the choice of pump frequency. To design an amplifier with a given bandwidth β, the pump frequency should be chosen so $\omega_o^2 >> \omega_D\beta$ in order to make $\beta_D >> \beta$. Then the varactor should be loaded at pump frequency such that $G_D = G_L$. By this technique, the following optimum low-frequency gain can be obtained:

$$(TG)_{0|\ max} = \frac{2\alpha\omega_D}{\beta} \tag{67}$$

The maximum value of voltage-gain-times-bandwidth is now

$$(GB)_{MAX} = (2\pi)^{-1} \sqrt{2\alpha\omega_D\beta} \tag{68}$$

By comparing (68) with (57) the effect of varactor losses is quite evident. If $\omega_p = a\sqrt{\beta\omega_D}$, then α must be at least α^2 times larger with varactor loss than without to yield the same gain-bandwidth product. However, little advantage results from choosing (a) in excess of 3, which limits the usefulness of arbitrarily raising the pump frequency.

Returning to the example at the end of Section 4, the effects of varactor loss will now be illustrated by assuming a varactor with cutoff frequency $\omega_D = 2\pi(10^5\ \text{Mc})$. To retain a 20-db gain and 100-Mc bandwidth with minimum pumping (i.e., minimum α) it is necessary that

$$\omega_p >> \sqrt{\beta\omega_D} = 2\pi(3\cdot3\cdot10^3\ \text{Mc})$$

Choosing $\omega_p = 2\pi(10^4\ \text{Mc})$ yields (by 64)

$$\beta_D = 2\pi(500\ \text{Mc})$$

Letting $G_L = G_D$, so

$$\beta_o = \beta_D + \beta_L = 2\pi(1000\ \text{Mc}) ,$$

then by (66)

$$\frac{2\pi}{\beta_s} = \frac{1}{100 \text{ Mc}} - \frac{1}{1000 \text{ Mc}} = \frac{1}{110 \text{ Mc}}$$

and by (66)

$$\alpha = \frac{(100)(110 \text{ Mc})}{2 \cdot 10^5 \text{ Mc}} = 0.05$$

which is some five times larger than the α predicted in the absence of varactor loss. (Note: in addition, the previous calculation assumed a pump frequency only half as large.) Since the value 0.05 is half the safe upper limit assumed for α, it will be concluded that 20 db gain is an upper limit for a Brett amplifier with a 100 Mc bandwidth and employing a varactor with 10^5 cut off frequency.

5.3 Noise Figures

Because the active element in the Brett amplifier is reactive (i.e., a pumped, nonlinear capacitance), it might be anticipated that negligible excess noise would be associated with it. However, in other types of reactive mixers (e.g., parametric amplifiers) thermal noise associated with parasitic resistance in the varactor element provides the lower limit for excess noise. In addition, negative resistance tends to be reflected at various sideband frequencies, which causes the reactive mixer to accentuate external circuit noise. It is important to examine the Brett circuit for these types of noise mechanisms.

Considering the diagram in Fig. 5, it is evident that excess noise can arise in both the video band and the pump pass band. In the latter, thermal noise will come from the varactor loss (G_D) and the load (G_L). Normally load noise would not be held against the amplifier, but

analysis will show that the pump accentuates load noise in this circuit, so the load is a source of excess noise. In the video band, excess noise will come primarily from parasitic losses in cables and transformers, etc., since varactor loss can be neglected at the rather low signal frequencies involved (i.e., $\omega_s << \omega_p$). Therefore, no excess noise will be attributed to the varactor in the video band.# With these assumptions, the noise figure of the Brett amplifier can be expressed by

$$F = 1 + \frac{N_s + N_o}{KTB_N(TG)_o} \tag{69}$$

where

N_s = output noise power due to parasitic losses in video input circuit

N_o = excess output noise power due to pump tank losses and the output load

T = room temperature

B_N = amplifier noise bandwidth in cps

If G_s' is the effective parasitic conductance of the video input circuit, and G_{so} is the video source conductance ($G_s = G_{so} + G_s'$), then

$$\frac{N_s}{KTB_N(TG)_o} = \frac{G_s'}{G_{so}}$$

if G_s' and G_{so} are at room temperature. By careful design, G_s'/G_{so} should be small, but the actual value of G_s' could depend on numerous external factors. No attempt will be made to evaluate N_s numerically.

The more fundamental noise source is N_o, which depends upon the varactor. To calculate N_o, first consider an increment of the pump cir-

---

#Although the preceding analysis has been applied for $0 < f_s <$ hundreds of megacycles, the use of input transformers will generally limit the lower value of f_s (to say 0.1 Mc), so nonthermal, low-frequency noise mechanisms will be neglected in this report.

cuit pass band lying between ω_1 and $\omega_1 + d\omega_s$, as diagramed in Fig. 13. Due to thermal noise arising from the pump conductance G, each such increment of the pump pass band will experience an incident RMS noise current

$$di_N = \sqrt{\frac{4KT' G d\omega_s}{2\pi}} \tag{70}$$

where

$$T' = \frac{T_L G_L + T_D G_D}{G_L + G_D}$$

is the noise temperature of the parallel combination of G_L and G_D, assuming the individual noise temperatures are T_L and T_D, respectively. This incident noise current will contribute to output noise in two ways, by noise reflected in each $d\omega_s$ increment, and by noise converted from the image increment lying between ω_{-1} and $\omega_{-1} - d\omega_s$. To evaluate these two noise contributions, which will be assumed to be uncorrelated, let

$Y_{1_{IN}}$ = input admittance at ω_1

$Y_{-1_{IN}}$ = input admittance at ω_{-1}

$Y_{1,-1}$ = transfer admittance from ω_{-1} to ω_1

$Y_{-1,1}$ = transfer admittance from ω_1 to ω_{-1}

The total output noise power in the increment $d\omega_s$ in Fig. 13 now becomes

$$P(\omega_s)\, d\omega_s = \frac{|di_N|^2 G}{|Y_{1_{IN}}|^2} + \frac{|di_N|^2 G}{|Y_{1,-1}|^2} \tag{71}$$

By assuming ω_o constant and treating ω_s as the variable, (71) expresses the noise power distribution over the right half of Fig. 13.

But from (47) and (48),

$$Y_{1_{IN}}(\omega_s) = Y^*_{-1_{IN}}(-\omega_s) = \frac{Y_1\left(Y_s Y_1 + 2\omega_s^2 \left|\frac{C_o}{2}\right|\right)}{Y_1 Y_s - \omega_s(\omega_o-\omega_s)\left|\frac{C_o}{2}\right|^2} \tag{72a}$$

$$Y_{1,-1}(\omega_s) = Y^*_{-1,1}(-\omega_s) = \frac{-Y_1\left(Y_s Y_1 + 2\omega_s^2 \left|\frac{C_o}{2}\right|^2\right)}{\omega_s(\omega_o+\omega_s)\left|\frac{C_o}{2}\right|^2} \tag{72b}$$

and so (71) is valid over the left half of Fig. 13 when ω_s is negative.

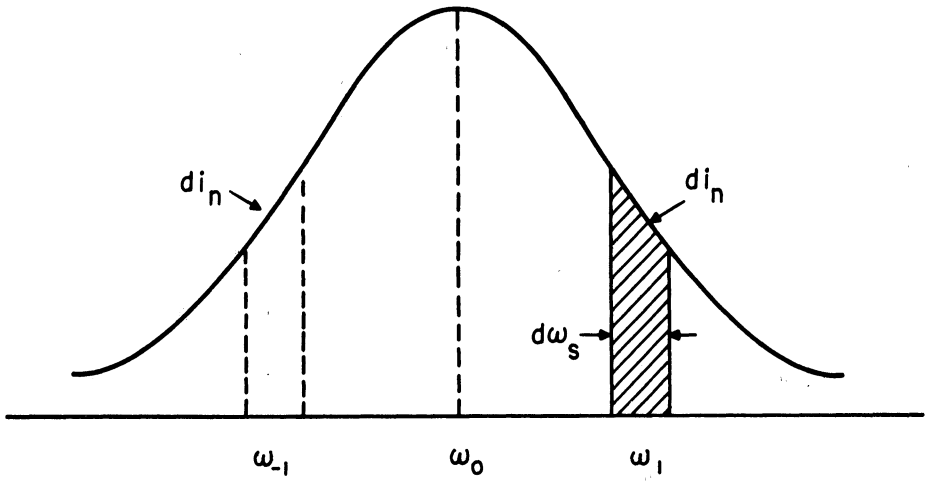

Fig. 13. Noise contributions from pump circuit conductance.

The total noise power delivered to G, P_G, can be found by integrating (71) for $-\infty \leq \omega_s \leq \infty$. If $\omega_s \ll \omega_o$ and $\alpha \ll 1$, it is shown in Appendix 2 that P_G can be expressed approximately by

$$P_G \approx \int_{-\infty}^{\infty} d\omega_s \left(\frac{4\alpha T'}{2\pi}\right)\left(\frac{1}{1+\frac{\omega_s^2}{\beta_o^2}}\right)\left[1 + \frac{\frac{1}{2}\left(\frac{\alpha\,\omega_s\omega_o}{\beta_s\,\beta_o}\right)^2}{\left(1-\frac{\omega_s^2}{\beta_s\beta_o}\right)^2 + \omega_s^2\left(\frac{1}{\beta_s}+\frac{1}{\beta_o}\right)^2}\right] \tag{73}$$

The effects of pumping on load noise are now evident through the term in (73) containing α. Since α vanishes in the absence of pumping, this term

will be the excess load noise that must be held against the amplifier.

The quantitative evaluation of (73) is carried out in Appendix 2 for the condition where $\beta_o >> \beta_s$. This case has been chosen because it was previously shown to yield maximum gain in the presence of varactor loss. Denoting the total noise power reaching the external load (G_L) by P_{G_L}, (73) now yields

$$P_{G_L} \approx \left(\frac{G_L}{G_L + G_D}\right)\left[4KT'\left(\frac{2\beta_o}{2\pi}\right)\left(\frac{\pi}{2}\right)\left(1 + \frac{\alpha^2\omega_o^2}{4\beta_o\sqrt{\beta_s\beta_o}}\right)\right] \tag{74}$$

Therefore

$$N_o = \left(\frac{G_L}{G_L + G_D}\right)\left(4KT'B_{o_N}\right)\left(\frac{\alpha^2\,\omega_o^2}{4\beta_o\sqrt{\beta_s\beta_o}}\right)$$

where

$$B_{o_N} = \frac{\pi}{2}\left(\frac{2\beta_o}{2\pi}\right)$$

is the noise bandwidth of the pump circuit in cps, as can be identified by comparing the first term in (74) with (69).

Again concentrating on the adjustments associated with optimum gain, as discussed in Section 5.2, let $G_L = G_D$ so $\beta_o = \omega_o^2/\omega_D$ (by 63), then

$$N_o = \frac{1}{2}\left(4KT'B_{o_N}\right)\left(\frac{\alpha^2\,\omega_D}{4\sqrt{\beta_s\beta_o}}\right) \tag{75a}$$

or, by (66), and noting that $\beta_s \approx \beta$,

$$N_o = \frac{1}{2}\left(4KT'B_N\right)\frac{\alpha(TG)_o}{8}\sqrt{\frac{\beta_o}{\beta}} \tag{75b}$$

Therefore, by (69), the basic contribution of the varactor to the amplifier noise figure will be

$$\boxed{F + 1 + \frac{\alpha}{16}\sqrt{\frac{\beta_o}{\beta}}\,\frac{T'}{T}} \qquad (76)$$

In the practical example in Section 5.2, design considerations were given for obtaining a 1000-Mc gain-bandwidth product, using a varactor with a 10^5-Mc cut-off frequency. This design called for $\alpha = 0.05$, $\beta_o \approx 10\,\beta$, and $(TG)_0 = 100$; so, by (75b), the load noise power is approximately doubled through the action of the pump. However, if $T' = T$, this excess power contributes less than 0.1 db to the circuit noise figure in (76). This extremely low varactor noise figure occurs primarily because of the choice of the operating frequencies. The close spacing and equal loading of the output sidebands greatly suppresses the undesirable, negative resistance effects due to the lower sideband effects that are well known in conventional single-sideband parametric amplifiers. The moderate enhancement of output load noise that is predicted by (75b) contributes very minutely to noise figure, since excess output noise contributes to F in proportion to the inverse of $(TG)_0$, and $(TG)_0$ is large by virtue of the high $\frac{\omega_o}{\beta}$ ratio.

If measured noise figures exceed the numerical values predicted above, experiments will have to determine the source of additional noise contributions. For example, concern must be given for the effective load noise temperature T'. While the varactor can be assumed to be at room temperature ($T_D = T$), the load temperature T_L may be much larger, since pump oscillator noise will contribute to T_L. If this effect is large, pump oscillator padding will be required to reduce T_L.

Another contribution to T_L will be the load temperature itself. If this is large compared to room temperature, it can be reduced with the aid of a nonreciprocal device such as an isolator or circulator. Finally,

the magnitude of input circuit noise must be estimated in an actual circuit, so it can be included in (76) according to (69). But these extraneous effects are largely under the control of the circuit designer, so very low noise figures can generally be expected from the Brett circuit.

6. CONCLUSION

In spite of the complexity of the analysis in this report, the Brett amplifier is a simple, and effective, circuit. It is capable of gain-bandwidth products that surpass those of the best vacuum tubes and most transistors. In addition, the Brett circuit is capable of noise figures that are significantly lower than are provided by these more conventional components.

It has been determined that the Brett circuit operates by allowing an input (video) signal to phase-modulate a carrier (pump) by means of a nonlinear reactive element (varactor). Amplification is possible because the pump and signal, respectively, contribute power to the modulation process approximately according to the ratio

$$\left(\frac{\text{pump frequency}}{\text{signal frequency}}\right)^2$$

An amplified version of the input signal can thus be obtained by detecting the modulated carrier with an efficient phase detector. An additional advantage of the Brett circuit is its positive input resistance at the video frequency.

For an ideal circuit, with fixed pump frequency, optimum gain occurs when the bandwidths of the pump and video circuits are in the ratio 2:1, respectively. However, for optimum transducer gains it is essential to control these bandwidths with minimum shunt capacity. For this reason, input transformers are useful for controlling the video bandwidths.‡

When varactor losses are considered, a useful upper limit in pump frequency occurs because the above bandwidth rule cannot be satis-

‡In this connection, several simple, ultra-wideband transformers have recently been constructed by this laboratory and will be the subject of a future report.

fied at high pump frequencies. To obtain optimum gain in this case, the pump frequency must be raised until the pump bandwidth is much larger than the video bandwidth, so the amplifier bandwidth can be determined entirely by the video circuit.

Since varactor losses will also provide the ultimate limitation on noise figures, a noise analysis has been made for the case where varactor loss is significant. Noise figure formulas were derived, and an illustrative calculation was made for an amplifier with a 1000-Mc gain-bandwidth product. It was shown that a varactor with a 10^5-Mc cut-off frequency would contribute less than 0.1 db to the total amplifier noise figure. These results are generally consistent with the experimental results reported to date by Brett and others (private communications).

APPENDIX I

The analysis of Section 3 assumes that all extraneous sidebands are short-circuited. However, this assumption is unnecessary if $|V_s| \ll |V_o|$ To prove this statement, the voltage components calculated by (47), due to I_{so}, can be used to find the components of short-circuit current in (41). For example, if I_{2s} is the complex Fourier component of short-circuit current at $2\omega_s$, then by (40)

$$I_{2s} = 2j\omega_s V_1 V^*_{-1}$$

and by (45a) and (48a)

$$\frac{I_{2s}}{I_{so}} = \left[\frac{j\omega_s C_p V_1 V^*_{-1}}{Y_{S_{IN}} V_s^2}\right]\left[\frac{V_s}{V_o}\right]$$

Since the factor in the first bracket is independent of V_s, the short-circuit current available to the video circuit, at the video harmonic, will be small compared to the applied video current when $|V_s| \ll |V_o|$. as similar conclusion can be reached for the other components of short-circuit current in (41). Therefore, for small signals, the assumptions stated at the beginning of Section 3 are valid.

APPENDIX II

The derivation of (73) and (74) proceeds as follows. Letting

$$p = \frac{\omega_s}{\sqrt{\beta_s \beta_o}} \; ; \; q = \frac{\omega_o}{\sqrt{\beta_s \beta_o}} \; ; \; \mu = \sqrt{\frac{\beta_s}{\beta_o}} + \sqrt{\frac{\beta_o}{\beta_s}} \tag{77}$$

then (72a) and (72b) become

$$|Y_{1_{IN}}|^2 = G^2 \left(1 + \frac{\beta_s}{\beta_o} p^2\right) \left| \frac{1 - p^2 + \alpha p^2 + j\, pu}{1 - p^2 - \frac{1}{2} p(q - p)\alpha + j\, pu} \right|^2 \tag{78a}$$

$$|Y_{1,-1}|^2 = G^2 \left(1 + \frac{\beta_s}{\beta_o} p^2\right) \left| \frac{1 - p^2 + \alpha p^2 + j\, pu}{\frac{1}{2} p(q + p)\, \alpha} \right|^2 \tag{78b}$$

When these equations are combined to form (71), terms of odd symmetry in ω_s (or x) can be dropped, since the integral of (71) is desired. The noise power delivered to G, P_G, now becomes

$$\int_{-\infty}^{\infty} P(\omega_s) d\omega_s = \frac{4KT'}{2\pi} \int_{-\infty}^{\infty} \frac{\beta_s \beta_o \, dp}{\left(1 + \frac{\beta_s}{\beta_o} p^2\right)}$$

$$\left\{ \frac{[1 - p^2(1 - \frac{\alpha}{2})]^2 + (pu)^2 + (\frac{\alpha}{2} p)^2 (p^2 + 2q^2)}{[1 - p^2 (1 - \alpha)]^2 + (pu)^2} \right\}$$

and if $\alpha \ll 1$ and $p^2 \ll q^2$, this relation can be reduced to

$$P_G = \frac{4KT'}{2\pi} \int_{\infty}^{\infty} \frac{\sqrt{\beta_s \beta_o}\, dp}{\left(1 + \frac{\beta_s}{\beta_o} p^2\right)} \left[1 + \frac{\frac{1}{2}(\alpha pq)^2}{(1 - p^2)^2 + (pu)^2}\right] \qquad (79)$$

which is equivalent to (73).

When (79) is integrated term by term, the first term yields (Dwight 120.01)

$$\frac{4KT'}{2\pi} \int_{-\infty}^{\infty} \frac{\sqrt{\beta_s \beta_o}\, dp}{\left(1 + \frac{\beta_s}{\beta_o} p^2\right)} = \left(\frac{4KT'}{2\pi}\right)\left(\pi\beta_o\right) \qquad (80)$$

In the second term,

$$(1 - p^2)^2 + (pu)^2 \approx \left(p^2 + \frac{1}{u^2}\right)(p^2 + u^2 - 2)$$

if $u^2 > 4$. Therefore, for the case where $\beta_s \gg \beta_s$, so that $u^2 \approx \frac{\beta_o}{\beta_s} \gg 1$, the second term in (80) becomes approximately (Dwight 120.2).

$$\left(\frac{4KT'}{2\pi}\right)\sqrt{\beta_s\beta_o} \int_{-\infty}^{\infty} \frac{\frac{1}{2}\left(\frac{\alpha q}{u}\right)^2 dp}{\left(1 + \left(\frac{p}{u}\right)^2\right)^2} = \left(\frac{4KT'}{2\pi}\right)(\alpha q)^2 \left(\frac{\pi}{4u}\right)\sqrt{\beta_s\beta_o} \qquad (81)$$

Equation 74 can now be obtained directly from (80) and (81). It should be noted that the approximations made in obtaining (81) introduce positive errors, so (74) is a slightly conservative estimate of output noise power.

REFERENCES

1. J. M. Manley and H. E. Rowe, "Some General Properties of Nonlinear Elements - Part I. General Energy Relations," Proc. IRE, Vol. 44, pp. 904-913, July 1956.

2. H. E. Rowe, "Some General Properties of Nonlinear Elements - Part II. Small Signal Theory," Proc. IRE, Vol. 46, No. 5, May 1958, pp.850-860.

3. K. Kurrokawa and M. Uenohara, "Minimum Noise Figure of the Variable-Capacitance Amplifier," BSTJ, Vol. XL, No. 3, May 1961, pp. 695-722.

4. D. K. Adams, "An Analysis of Four-Frequency Nonlinear Reactance Circuits," IRE Transactions on Microwave Theory and Techniques, Vol. MTT-8, No. 3, May 1960, pp. 274-283. (See also, D. K. Adams,"Some Considerations of Four-Frequency Nonlinear Reactance Circuits," Cooley Electronics Laboratory Technical Report No. 96, The University of Michigan, September 1959.)

5. H. Brett, F. A. Brand, W. G. Matthei, "A Varactor Diode Parametric Standing-Wave Amplifier," Proc. IRE, Vol. 49, No. 2, February 1961, pp. 509-510.

6. L. Blackwell and K. Kotzebue, "Semiconductor-Diode Parametric Amplifiers," Prentice-Hall, Inc., 1961.

DISTRIBUTION LIST

Unclassified Distribution List - Contract DA 36-039 sc-78283

Copy No.	
1-27	Commanding Officer, U. S. Army Signal Research and Development Laboratory, Fort Monmouth, New Jersey, ATTN: Senior Scientist, Countermeasures Division
28	Commanding General, U. S. Army Electronic Proving Ground, Fort Huachuca, Arizona, ATTN: Director, Electronic Warfare Dept.
29	Chief, Research and Development Division, Office of the Chief Signal Officer, Dept. of the Army, Washington 25, D. C., ATTN: SIGEB
30	Commanding Officer, Signal Corps Electronic Research Unit, 9560th USASRU, P. O. Box 205, Mountain View, California
31	U. S. Atomic Energy Commission, 1901 Constitution Avenue, N. W., Washington 25, D. C., ATTN: Chief Librarian
32	Director, Central Intelligence Agency, 2430 E Street, N. W., Washington 25, D. C. ATTN: OCD
33	Signal Corps Liaison Officer, Lincoln Laboratory, Box 73 Lexington 73, Massachusetts, ATTN: Col. Clinton W. Janes
34-43	Commander, Armed Services Technical Information Agency, Arlington Hall Station, Arlington 12, Virginia
44	Commander, Air Research and Development Command, Andrews Air Force Base, Washington 25, D. C., ATTN: SCRC, Hq.
45	Directorate of Research and Development, USAF, Washington 25, D. C., ATTN: Chief, Electronic Division
46-47	Hqs., Aeronautical System Division, Air Force Command, Wright Patterson Air Force Base, Ohio, ATTN: WWAD
48	Hqs., Aeronautical System Division, Air Force Command, Wright Patterson Air Force Base, Ohio, ATTN: WCLGL-7
49	Hqs., Aeronautical System Division, Air Force Command, Wright Patterson Air Force Base, Ohio - For retransmittal to - Packard Bell Electronics, P. O. Box 337, Newbury Park, California
50	Commander, Air Force Cambridge Research Center, L. G. Hanscom Field, Bedford, Massachusetts, ATTN: CROTLR-2
51-52	Commander, Rome Air Development Center, Griffiss Air Force Base, New York, ATTN: RCSSLD - For retransmittal to - Ohio State University Research Foundation
53	Commander, Air Proving Ground Center, ATTN: Adj/Technical Report Branch, Eglin Air Force Base, Florida
54	Commander, Special Weapons Center, Kirtland Air Force Base, Albuquerque, New Mexico
55	Chief, Bureau of Naval Weapons, Code RRR-E, Department of the Navy, Washington 25, D.C.
56	Chief of Naval Operations, EW Systems Branch, OP-35, Department of the Navy, Washington 25, D. C.
57	Chief, Bureau of Ships, Code 691C, Dept. of the Navy, Washington 25, D. C.
58	Chief, Bureau of Ships, Code 684, Dept. of the Navy, Washington 25, D. C.
59	Chief, Bureau of Naval Weapons, Code RAAV-33, Department of the Navy, Washington 25, D.C.
60	Commander, Naval Ordnance Test Station, Inyokern, China Lake, California, ATTN: Test Director - Code 30
61	Director, Naval Research Laboratory, Countermeasures Branch, Code 5430, Washington 25, D. C.
62	Director, Naval Research Laboratory, Washington 25, D. C., ATTN: Code 2021
63	Director, Air University Library, Maxwell Air Force Base, Alabama, ATTN: CR-4987
64	Commanding Officer - Director, U. S. Naval Electronic Laboratory, San Diego 52, Cal.
65	Office of the Chief of Ordnance, Department of the Army, Washington 25, D. C., ATTN: ORDTU
66	Chief, West Coast Office, U. S. Army Signal Research and Development Laboratory, Bldg. 6, 75 S. Grand Avenue, Pasadena 2, Cal.
67	Commanding Officer, U. S. Naval Ordnance Laboratory, Silver Springs 19, Maryland
68-69	Chief, U. S. Army Security Agency, Arlington Hall Station, Arlington 12, Virginia, ATTN: IADEV
70	President, U. S. Army Defense Board, Headquarters, Fort Bliss, Texas
71	President, U. S. Army Airborne and Electronics Board, Fort Bragg, North Carolina
72	U. S. Army Antiaircraft Artillery and Guided Missile School, Fort Bliss, Texas
73	Commander, USAF Security Service, San Antonio, Texas, ATTN: CLR
74	Chief, Naval Research, Department of the Navy, Washington 25, D. C., ATTN: Code 931

Copy No.	
75	Commanding Officer, U. S. Army Security Agency, Operations Center, Fort Huachuca, Arizona
76	President, U. S. Army Security Agency Board, Arlington Hall Station, Arlington 12, Virginia
77	Operations Research Office, John Hopkins University, 6935 Arlington Road, Bethesda 14, Maryland, ATTN: U. S. Army Liaison Officer
78	The John Hopkins University, Radiation Laboratory, 1315 St. Paul Street, Baltimore 2, Maryland, ATTN: Librarian
79	Stanford Electronics Laboratories, Stanford University, Stanford, California, ATTN: Applied Electronics Laboratory Document Library
80	HRB Singer, Inc., Science Park, State College, Pennsylvania, ATTN: R. A. Evans, Manager, Technical Information Center
81	ITT Laboratories, 500 Washington Avenue, Nutley 10, New Jersey, ATTN: Mr. L. A. DeRosa, Div. R-15 Lab.
82	Director, USAF Project Rand, via Air Force Liaison Office, The Rand Corporation, 1700 Main Street, Santa Monica, California
83	Stanford Electronics Laboratories, Stanford University, Stanford, California, ATTN: Dr. R. C. Cumming
84	Willow Run Laboratories, The University of Michigan, P. O. Box 2008, Ann Arbor, Michigan, ATTN: Dr. Boyd
85	Stanford Research Institute, Menlo Park, California, ATTN: Dr. Cohn
86	Stanford Research Institute, Menlo Park, California, ATTN: Dr. E. M. Jones
87-88	Commanding Officer, U. S. Army Signal Missile Support Agency, White Sands Missile Range, New Mexico, ATTN: SIGWS-EW and SIGWS-FC
89	Commanding Officer, U. S. Naval Air Development Center, Johnsville, Pennsylvania, ATTN: H. Bicking
90	Commanding Officer, U. S. Army Signal Research and Development Laboratory, Fort Monmouth, New Jersey, ATTN: U. S. Marine Corps Liaison Office, Code AO-4C
91	President, U. S. Army Signal Board, Fort Monmouth, New Jersey
92-100	Commanding Officer, U. S. Army Signal Research and Development Laboratory, Fort Monmouth, New Jersey ATTN: 1 Copy - Director of Research 1 Copy - Technical Documents Center ADT/E 1 Copy - Chief, Countermeasures Systems Branch, Countermeasures Division 1 Copy - Chief, Detection and Location Branch, Countermeasures Div. 1 Copy - Chief, Jamming and Deception Branch, Countermeasures Div. 1 Copy - File Unit No. 2, Mail and Records, Countermeasures Division 3 Cys - Chief, Security Division, (for retransmittal to BJSM)
101	Director, National Security Agency, Fort George G. Meade, Maryland, ATTN: TEC
102	Dr. B. F. Barton, Director, Cooley Electronics Laboratory, The University of Michigan, Ann Arbor, Michigan
103-124	Cooley Electronics Laboratory Project File, The University of Michigan, Ann Arbor, Michigan
125	Project File, The University of Michigan Office of Research Administration, Ann Arbor, Michigan

Above distribution is effected by Countermeasures Division, Surveillance Department, USASRDL, Evans Area, Belmar, New Jersey. For further information contact Mr. I. O. Myers, Senior Scientist, Telephone 59-61252.